Hospitalisation for COVID-19 predicts long lasting cerebrovascular impairment: A prospective observational cohort study

Kamen A. Tsvetanov [a,b,*], Lennart R.B. Spindler [a,c], Emmanuel A. Stamatakis [a,c], Virginia F.J. Newcombe [c,d], Victoria C. Lupson [c,d], Doris A. Chatfield [c], Anne E. Manktelow [c], Joanne G. Outtrim [c], Anne Elmer [e], Nathalie Kingston [f,g], John R. Bradley [f,h], Edward T. Bullmore [d,i,5], James B. Rowe [a,j,5], David K. Menon [c,d,e,h,5], The Cambridge NeuroCOVID Group[1], The NIHR COVID-19 BioResource[2], The Cambridge NIHR Clinical Research Facility[3], The CITIID-NIHR BioResource COVID-19 Collaboration[4]

[a] Department of Clinical Neurosciences, University of Cambridge, Cambridge, United Kingdom
[b] Department of Psychology, University of Cambridge, Cambridge, United Kingdom
[c] Division of Anaesthesia, Department of Medicine, University Cambridge, Cambridge, United Kingdom
[d] Wolfson Brain Imaging Centre, University of Cambridge, Cambridge, United Kingdom
[e] Cambridge Clinical Research Centre, NIHR Clinical Research Facility, Cambridge University Hospitals NHS Foundation Trust, Addenbrooke's Hospital, Cambridge, United Kingdom
[f] NIHR BioResource, Cambridge University Hospitals NHS Foundation, Cambridge Biomedical Campus, Cambridge, United Kingdom
[g] Department of Haematology, School of Clinical Medicine, University of Cambridge, Cambridge Biomedical Campus, Cambridge, United Kingdom
[h] Department of Medicine, University of Cambridge, Addenbrooke's Hospital, Cambridge, United Kingdom
[i] Department of Psychiatry, University of Cambridge, Cambridge Biomedical Campus, Cambridge, United Kingdom
[j] Medical Research Council Cognition and Brain Sciences Unit, Department of Psychiatry, Cambridge, United Kingdom

* Corresponding author at: Department of Clinical Neurosciences, University of Cambridge, Cambridge, United Kingdom.
 E-mail address: kat35@cam.ac.uk (K.A. Tsvetanov).

ARTICLE INFO

ABSTRACT

Human coronavirus disease 2019 (COVID-19) due to severe acute respiratory syndrome coronavirus-2 (SARS-CoV-2) has multiple neurological consequences, but its long-term effect on brain health is still uncertain. The cerebrovascular consequences of COVID-19 may also affect brain health. We studied the chronic effect of COVID-19 on cerebrovascular health, in relation to acute severity, adverse clinical outcomes and in contrast to control group data. Here we assess cerebrovascular health in 45 patients six months after hospitalisation for acute COVID-19 using the resting state fluctuation amplitudes (RSFA) from functional magnetic resonance imaging, in relation to disease severity and in contrast with 42 controls. Acute COVID-19 severity was indexed by COVID-19 WHO Progression Scale, inflammatory and coagulatory biomarkers. Chronic widespread changes in frontoparietal RSFA were related to the severity of the acute COVID-19 episode. This relationship was not explained by chronic cardiorespiratory dysfunction, age, or sex. The level of cerebrovascular dysfunction was associated with cognitive, mental, and physical health at follow-up. The principal findings were consistent across univariate and multivariate approaches. The results indicate chronic cerebrovascular impairment following severe acute COVID-19, with the potential for long-term consequences on cognitive function and mental wellbeing.

1. Introduction

Severe acute respiratory syndrome coronavirus-2 (SARS-CoV-2) causes human coronavirus disease 2019 (COVID-19) with multi-system effects that include neurological, vascular and neurovascular injury. Acute neurological sequelae are common, ranging from mild dizziness, headaches and anosmia to severe encephalitis, stroke and delirium (Chen et al., 2021; Hensley et al., 2022; Paterson et al., 2020; Zubair et al., 2020). These sequelae may arise from systemic physiological insults (e.g. hypoxia, hypotension, dysautonomia), coagulation dysfunction, large vessel occlusion, arterial stiffness, impaired vasoreactivity, neurotropic infection, parenchymal haemorrhage, or autoimmune responses against diverse antigens (Chen et al., 2021; Marcic et al., 2021; Mohkhedkar et al., 2021; Schnaubelt et al., 2021). Acute COVID-19 has also been associated with microvascular injury from vasculitis or endotheliitis (McGonagle et al., 2021a; McGonagle et al., 2021b), with endotheliopathy (Kakarla et al., 2021), vasogenic oedema and microthrombosis in the acute phase (Iba et al., 2020; Levi et al., 2020) and hypoperfusion in the subacute phase (Hosp et al., 2021). While this acute pathophysiology is detectable using neuroimaging (Hanafi et al., 2020; Lersy et al., 2021; Newcombe et al., 2021), the persistence and effects of cerebrovascular dysfunction over the medium- and long-term remain unknown.

An important aspect of cerebrovascular function is the capacity of cerebral vessels to constrict or dilate in response to physiological conditions such as alterations in carbon dioxide (CO_2) and oxygen tension. This cerebrovascular reactivity (Willie et al., 2014) regulates regional blood flow via pH-dependent modulation of vascular smooth muscle tone (Ainslie et al., 2005; Jensen et al., 1988; Lambertsen et al., 1961; Lassen, 1968), but is compromised by arterial stiffness, compromised endothelial function (Brandes et al., 2005), or disorders including hypertension, traumatic brain injury and dementia. Poor cerebrovascular reactivity may also increase the risk of neurodegeneration (Gao et al., 2013).

We therefore assessed the impact of COVID-19 on chronic cerebrovascular reactivity after hospitalisation. We used a well-established non-invasive imaging method, exploiting naturally occurring fluctuations in arterial CO_2 induced by variations in cardiac and respiratory cycles, which moderate the blood oxygenation level-dependent (BOLD) signal underlying functional magnetic resonance imaging (Birn et al., 2006; Glover et al., 2007). The BOLD signal variability at rest, known as resting state fluctuation amplitudes (RSFA), is a safe, scalable and robust alternative to the gold standard approaches of measuring cerebrovascular reactivity with MRI (Golestani et al., 2016; Kannurpatti and Biswal, 2008; Liu et al., 2017; Tsvetanov et al., 2021b; Tsvetanov et al., 2021c; Tsvetanov et al., 2015). It is easier and safer to apply in clinical cohorts than experimental hypercapnia, breath-holding and drug

interventions (Keyeux et al., 1995; Rostrup et al., 1996, 1994; Wagerle and Mishra, 1988). RSFA is sensitive to cerebrovascular and cardiovascular differences in ageing (Tsvetanov et al., 2021b), cerebrovascular disorders (Liu et al., 2021; Secchinato et al., 2019; Taneja et al., 2019), small vessel disease (Makedonov et al., 2013a), stroke (Nair et al., 2017), Alzheimer's disease (Millar et al., 2020a), cognitive performance (Liu et al., 2022; Millar et al., 2020b; Millar et al., 2021; Millar et al., 2021) and the presence of brain tumours (Agarwal et al., 2019).

Combining acute and convalescent assessments with serology diagnosis, we report on the chronic effect of COVID-19 on RSFA as a marker of cerebral microvascular function, in relation to acute severity and in contrast to control group data. Acute disease severity was quantified by the COVID-19 WHO Progression Scale and blood biomarkers in patients hospitalised for COVID-19. We predicted that acute COVID-19 changes regional RSFA at follow up, in proportion to acute disease severity, over and above the effects of residual systemic cardiorespiratory impairment. A secondary hypothesis was that the level of RSFA abnormality would relate to worse functional, cognitive and mental dysfunction months after hospitalisation. We further examined the spatial correspondence between regional differences in RSFA and normative regional variations in neurotransmitters/receptors, brain energy consumption and cell-type distributions. We hypothesised that the physiological and genetic signature of COVID-19-related cerebrovascular impairment shapes the composition of cell-types, metabolism and vasoreactivity essential for neuronal homeostasis.

2. Methods

2.1. Participants

Patients were recruited through the NIHR COVID-19 BioResource, which received ethical approval from East of England – Cambridge Central Research Ethics Committee (REC 17/EE/0025), and provided written informed consent. Eligibility was based on admission to Addenbrooke's Hospital, Cambridge UK with a serological diagnosis of COVID-19 between 10th March 2020 and 31st July 2020, aged 18 years or older, attended for outpatient visits following discharge, and no contraindications to MRI. 489 patients were potentially eligible. Clinical data were obtained from inpatient electronic medical records, and from cardiorespiratory and neurological assessments at follow-up clinical and research visits at least 6 weeks following symptom onset. 45 patients consented to participate and had clinical, structural magnetic resonance imaging (MRI) and resting state functional MRI (fMRI) data of appropriate quality (see below). Age and sex matched, non-hospitalised, non-COVID-19 controls (n = 42) were recruited by word of mouth and through the Cambridge NIHR BioResource (https://bioresource.nihr.ac.uk/centres-programmes/bioresource-centre-cambridge/). Controls

were scanned with the same sequences, with data pooled over protocol-optimisation cohorts to match demographics (Cambridgeshire Research Ethics Committee 97/290 and REC 17/EE/0025, and Norfolk EE/0395 and a protocol approved by the Human Biology Ethics Committee of the Council of the School of Biological Sciences, University of Cambridge).

The study design and the principal data processing pipelines are summarised in Fig. 1.

2.2. Inpatient data: COVID-19 severity

The WHO COVID-19 11-point Progression scale was used during hospitalisation to provide a measure of disease severity with scores from 0 (non-infected) to 10 (dead) (Marshall et al., 2020). We also used blood biomarkers previously associated with COVID-19 severity including the most extreme values during hospitalisation on the following routine clinical blood tests: haematological cell counts (lowest platelets) (Wool and Miller, 2021); inflammatory and acute phase proteins (C-reactive protein, CRP, serum ferritin) (Luan et al., 2021) (interleukin-6, IL-6) (Group and Sterne, 2021; Ulhaq and Soraya, 2020); liver function tests (bilirubin) (Bangash et al., 2020); and blood coagulation markers (D-dimer, prothrombin time (PT) and activated partial thromboplastin time (APTT)) (Asakura and Ogawa, 2021; Iba et al., 2020; Levi et al., 2020). All blood-based measurements were positively skewed on natural scales and were log-transformed for closer approximation to Normal distributions before statistical analysis. For consistency in interpreting scores across blood assays, platelet counts were inverted (iPlatelets) so that higher scores represent lower counts. All variables were normalised to a mean of 0 and standard deviation of 1.

2.3. Clinical outpatient visit: Cardiorespiratory assessments

Cardiorespiratory measurements were collected during a clinical assessment at least 12 weeks after discharge from initial hospitalization with COVID-19 using Care Fusion Micro Spirometer (Care Fusion, San Diego, CA). Systolic and diastolic blood pressure (BPS and BPD) were measured in lying (or seated) and standing positions by automated sphygmomanometry. We calculated pulse pressure (BPS-BPD) and orthostatic intolerance (BPS lying – BPS standing). Lying and standing pulse pressure values were log-transformed for Normality prior to statistical analysis. Lung function test determined peak expiratory flow (PEF), forced expiratory volume in 1 s (FEV1), forced vital capacity (FVC) and FEV1/FVC ratio. Measurements were repeated in triplicate, with one minute rest between measurements and log-transformed for Normality prior to statistical analysis. Pulse oximetry was used to determine the heart rate and arterial oxygen saturation before and following a 6-minute walk test (du Bois et al., 2012; Crapo et al., 2012; Enright et al., 2003).

2.4. Research visit: neurological assessment

2.4.1. Image acquisition and pre-processing

Imaging data were acquired using a 3T Siemens Prisma*fit* System with a 32–/20-channel head-coil at the Wolfson Brain Imaging Centre (WBIC; https://www.wbic.cam.ac.uk). A 3D-structural MRI was acquired on each participant using a T1-weighted sequence (3D Magenetisation-Prepared Rapid Gradient-Echo, 3D MPRAGE) with the following parameters: repetition time (TR) = 2 ms; echo time (TE) =
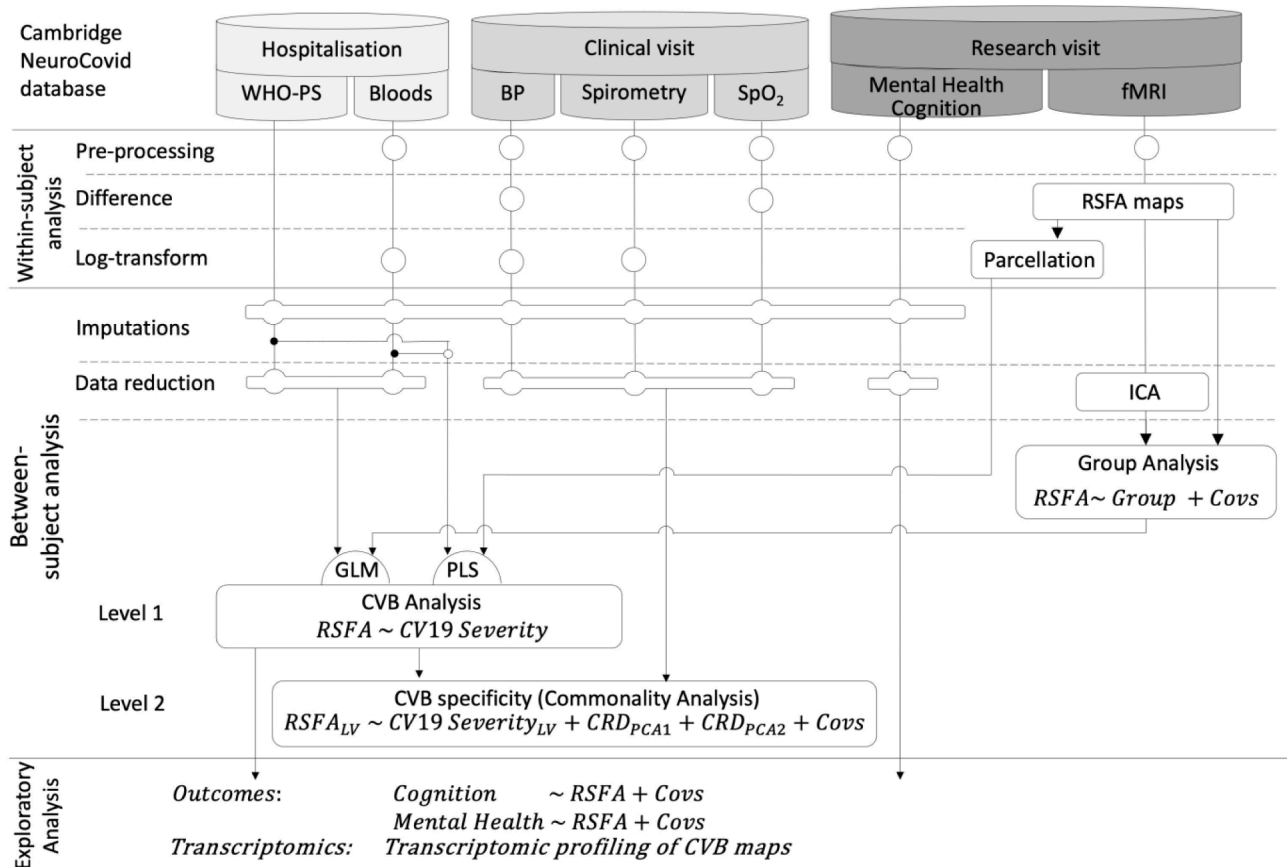
Fig. 1. Schematic representation of various modality datasets in the study, their processing pipelines on a within-subject level, as well as data-reduction techniques and analytical strategy on between-subject level to test for associations between acute COVID-19 Severity and chronic cerebrovascular impairment. WHO-PS, COVID-19 WHO progression scale; BP, blood pressure; SpO2, blood oxygen saturation; fMRI, functional magnetic resonance imaging; RSFA, resting state fluctuation amplitudes; PCA, principal component analysis; ICA, independent component analysis; Covs, covariates of no interest; GLM, general linear model; PLS, partial least squares; LV, latent variable from PLS analysis; CRD, cardiorespiratory dysfunction component; CVB, cerebrovascular burden;

2.99 ms; inversion time (TI) = 880 ms; flip angle α = 9°; field of view (FOV) = 208×256×256 mm3; resolution = 1 mm isotropic; accelerated factor (in-plane acceleration iPAT) = 2; acquisition time, 5 min. T1 images were pre-processed using SPM12. The T1 image was rigid-body coregistered to the MNI template, and segmented to extract probabilistic maps of five tissue classes: gray matter (GM), white matter (WM), CSF, bone, soft tissue and residual noise.

RSFA was estimated from resting state Echo-Planar Imaging (*EPI*) of 477 volumes acquired with 64 slices for whole brain coverage (TR = 735 ms; TE = 30 ms; FOV = 210 mm × 210mm; resolution = 2.38 × 2.38x2.4 mm) during 5 min and 51 s. Participants were instructed to lie still, to stay awake and keep their eyes open, looking at a fixation cross. *EPI* data preprocessing included the following steps: (1) temporal realignment of slices to (0,0,0) Montreal Neurological Institute (MNI) co-ordinates; (2) spatial realignment to adjust for linear head motion; (3) identification and censoring (scrubbing) of outlier scans using Artifact detection tools (ART, https://www.nitrc.org/projects/artifact_detect/); (4) rigid-body coregistration to the T1 anatomical image; and (5) application of the normalization parameters derived from T1 image coregistration to warp the functional images into MNI space. We applied whole-brain independent component analysis for single subject time series denoising to minimise motion artefacts using *a priori* heuristics implemented in the ICA-based Automatic Removal of Motion Artifact toolbox (Pruim et al., 2015b; Pruim et al., 2015a) after smoothing with a 6 mm FWHM Gaussian kernel.

RSFA maps were estimates using previously reported procedure (Tsvetanov et al., 2021b; Tsvetanov et al., 2015).To facilitate integrative multivariate analyses (see below), the RSFA maps were parcellated by a prior cortical template into 360 bilaterally symmetric regions (Glasser et al., 2016). Regional RSFA values were estimated by averaging over all voxels in each parcel.

2.4.2. Physical, cognitive and mental dysfunction (PMC)

Quality of life, cognition and mental health were assessed using a set of questionnaires: Generalised Anxiety Disorder-7 (GAD-7) (Spitzer et al., 2006; Swinson, 2006), Patient Health Questionnaire-9 (PHQ-9) (Kroenke et al., 2001), Patient Health Questionnaire-15 (PHQ-15) (Kroenke et al., 2002), Posttraumatic Stress Disorder Checklist-5 (PCL-5) (Blevins et al., 2015) and subscores from the Short Form-36 (SF-36) (Ware and Sherbourne, 1992). SF36 subscores were defined as physical functioning (SF36-PF), role limitation physical (SF36-RLP), role limitation emotional (SF36-RLE), energy dimension (SF36-ED), emotional wellbeing (SF36-EW), social functioning (SF36-SF), pain (SF36-P) and general health (SF36-GH).

Cognitive function and functional independence were evaluated using Montreal Cognitive Assessment (MOCA) (Nasreddine et al., 2005), inverted Modified Ranking Scale (iMRS) (Eriksson et al., 2007) and Barthel Index (BI) (Mahoney and Barthel, 1965). For consistency in interpreting scores across questionnaires, scores for mental health questionnaires were inverted (iGAD-7, iPHQ-9, iPHQ-15 and iPCL-5) so that lower values represent greater mental health problems.

2.5. Analytical approach

2.5.1. Group differences in cerebral microvascular health

To study differences in cerebral microvascular health between COVID-19 cases and controls, we performed independent component analysis on the imaging-based RSFA data to separate spatially overlapping sources of signal with different aetiologies (Xu et al., 2013), as it is known that cardiovascular versus cerebrovascular signals may vary across individuals and brain region in RSFA (Tsvetanov et al., 2021b). The independent component analysis was performed across participants to determine spatially non-overlapping RSFA maps without using group information, termed Source-Based Cerebrovasculometry (Tsvetanov et al., 2021b; Tsvetanov et al., 2015) with ICASSO (software for investigating the reliability of ICA estimates by clustering and visualisation;

Himberg and Hyvarinen, 2003) across 128 iterations using the Group ICA of fMRI Toolbox (https://mialab.mrn.org/software/gift/index.html; Calhoun et al., 2001). In brief, the fastICA algorithm was applied after the optimal number of sources explaining the variance in the data was identified using PCA with Minimum Description Length (MDL) criterion (Hui et al., 2011; Li et al., 2007; Rissanen, 1978). By combining the PCA and ICA, the concatenated RSFA maps in a *n*-by-m matrix of participants-to-voxels are decomposed into: (i) a set of maximally independent components, each characterized by a different, cerebrovasculometry source map, showing the spatial projection of the component to each brain voxel (termed $RSFA_{IC}$ maps), and (ii) the degree to which each participant expresses the spatial map of the corresponding component ($RSFA_{IC}$ map), termed subject scores. Subject scores for each component were predicted by diagnostic status (COVID-19 cases vs controls), age, and sex in a subsequent robust multiple linear regression. The regression model was specified by Wilkinson's notation, '$RSFA_{IC}$ ~ 1 + group*age + sex' and fitted for each component separately. Models were corrected for multiple comparisons at p < 0.05 (FDR-corrected). To confirm the validity of the results a univariate voxel-wise analyses was performed.

2.5.2. Linking COVID-19 severity to cerebrovascular impairment and their correlates

Rate of missing inpatient, outpatient and research visit data varied between 0 and 38 % (see Table 1); hence, to increase statistical power and efficiency, missing data were imputed before further statistical analyses (see below). Incomplete variables were imputed under fully conditional specification, using the default settings of the multivariate imputation by chained equations (MICE) in R (van Buuren and Groothuis-Oudshoorn, 2011). Multiple versions of each dataset were created (m = 5). Instead of accounting for variability in the parameter estimates between imputed datasets, we report any differences in the significance of parameters input to the multiple linear regression.

Statistical analyses used Matlab 2020b calling the packages as described below. Datasets of interest stemmed from a range of modalities and different time-points: i) inpatient blood samples, ii) outpatient cardiorespiratory dysfunction, iii) mental health and RSFA measures during a research visit. To make these datasets tractable for univariate stages of the two-level analytical procedure (Passamonti et al., 2019; Tsvetanov et al., 2021a; Tsvetanov et al., 2018; Tsvetanov et al., 2016). In the first-level analysis, the link between COVID-19 severity and RSFA data was identified using a multivariate approach (see below). In the second-level analysis, we tested whether the COVID-19-RSFA link can be explained by other variables of interest or potential covariates of no interest using regression-based analyses (see below). We therefore constructed a set of summary measures for each non-imaging modality (i.e. components, Fig. 1). This had two advantages. First, it reduced the number of statistical comparisons. Second, it improved interpretability of the signals in each modality data by means of denoising and simplification given; low-dimensional data representations remove noise but retain signal of interest that can be instrumental in understanding hidden structures and patterns of multivariate data. We performed principal component analysis as a widely used dimensionality reducing approach (Hotelling, 1933; Pearson, 1901; van der Maaten et al., 2009) on each set of non-imaging variables from clinical and research assessments data before integrating them with MRI data as described below. For this purpose, we used Matlab's function *pca.m* with default settings, where the number of components was determined using Horn's parallel analysis (Dobriban, 2020; Horn, 1965) using 10,000 permutations. All variables were normalised to a mean of 0 and standard deviation of 1 prior principal component analysis.

2.5.2.1. Chronic cardiorespiratory dysfunction. Cardiorespiratory dysfunction was represented by the first two principal components (CRD_{PC1} and CRD_{PC2}) constructed from blood pressure (lying and

Table 1

Characteristics of 45 cases hospitalised with COVID-19. n – indicates number of patients and the percentage of patients from the patient cohort (%), SD – standard deviation, IQR – interquartile range, kg – weight in kilograms, m – height in meters.

Variable	Patients	
	n (%)	Mean(SD)/Median(IQR)*
Age (years)	45 (100)	52 (14)
Education (years)	45 (100)	16 (4)
Female	26 (58)	–
Right-handed	40 (89)	–
Pre-existing comorbidies (n > 1)		
Cardiovascular	11 (24)	–
Respiraroty	8 (18)	–
Type-2 Diabetes	4 (9)	–
Hypothyroidism	4 (9)	–
Neurological	2 (4)	–
Inpatient data		
Vasopressors	10 (22)	–
Dialysis	4 (9)	–
BMI (kg/m2)	36 (80)	29 (4)
Mechanical Ventilation (days)	13 (29)	20 (15)
CRP	42 (93)	149 (147)
D Dimer	37 (82)	1125 (2071)
Ferritin	32 (71)	1225 (1700)
IL-6	28 (62)	39 (80)
PT	32 (71)	26 (54)
APTT	33 (73)	42 (36)
Bilirubin	43 (96)	14 (8)
Platelets	44 (98)	230 (102)
Clinical Visit		
HR (bpm)	38 (84)	76 (14)
RR (cpm)	38 (84)	16 (2)
SBP lying (mmHg)	38 (84)	134 (23)
SBP standing (mmHg)	33 (73)	130 (20)
DBP lying (mmHg)	38 (84)	74 (12)
DBP standing (mmHg)	33 (73)	79 (11)
Research Visit		
GAD-7 (0–21)	44 (98)	4 (8)*
PHQ-9 (0–27)	44 (98)	7 (9)*
PHHQ-15 (0–30)	39 (87)	9 (8)*
PCL-5 (0–80)	44 (98)	16 (22)*
MoCA	39 (87)	28 (3)*
mRS	39 (87)	1 (1)*
BI	37 (82)	20 (0)*
Initial symptoms to Admission (days)	40 (89)	14 (14)
Hospitalisation Duration (days)	40 (89)	19 (31)
Intial symptoms to Clinic visit (days)	39 (87)	169 (35)
Intial symptoms to Research visit (days)	45 (100)	180 (58)

standing pulse pressure, and orthostatic systolic and diastolic blood pressure), differences in heart rate and blood oxygenation during a 6-minute walk test, and a spirometry pulmonary function component.

2.5.2.2. Chronic physical, cognitive, and mental dysfunction (PCM). Chronic physical, cognitive and mental dysfunction (PCM) was represented by the first two principal components (PCM_{PC1} and PCM_{PC2}) constructed from mental health scores (GAD-7, PHQ-9, PHQ-15, and SF-36 sub-scores), cognitive function (MoCA) and functional independence measures (Barthel Index and imRS).

2.5.2.3. Two-level approach linking COVID-19 severity to cerebrovascular impairment and their correlates. The prediction of RSFA abnormality by prior clinical assessment of COVID-19 severity was tested using a multivariate approach using a two-level procedure (Passamonti et al.,

2019; Tsvetanov et al., 2021a; Tsvetanov et al., 2018; Tsvetanov et al., 2016). First, the relationships between COVID-19 severity and RSFA data were identified using partial least squares (Krishnan et al., 2011) of RSFA maps and COVID-19 Severity data, by providing pairs of latent variables ($RSFA_{LV}$) and (COVID-19 $Severity_{LV}$). Data set 1 consisted of parcellated RSFA maps across all patients (45 cases × 360 brain regions; RSFA dataset). Data set 2 included the COVID-19 WHO Progression scale and inpatient blood assay results (45 cases × 9 clinical severity measures; COVID-19 Severity dataset). All variables were Z-scored (mean of 0 and standard deviation of 1) before PLS with 10,000 random permutations of dataset 2 to determine the significance of the latent variables. To confirm the validity of the results, a univariate voxel-wise analyses was performed.

Second, we tested whether the identified relationship between COVID-19 $Severity_{LV}$ and $RSFA_{LV}$ could be explained by other variables of interest or potential confounding variables of no interest useing robust multiple linear regression and commonality analysis (Kraha et al., 2012; Nimon et al., 2008). Commonality analysis partitions the variance explained by all predictors in a multiple linear regression model into variance unique to each predictor and variance shared between each combination of predictors. Therefore, unique effects indicate the (orthogonal) variance explained by one predictor over and above that explained by other predictors in the model, while common effects indicate the variance shared between correlated predictors. Notably, the sum of variances, also known as commonality coefficients, equals the total proportion of variance explained $R2$ by the regression model. We adapted a commonality analysis algorithm (Nimon et al., 2008) implemented in Matlab (Wu et al., 2023). This model tested whether the relationship between COVID-19 $Severity_{LV}$ and $RSFA_{LV}$ can be explained partly or fully by systemic cardiorespiratory dysfunction or other covariates of no interest. The regression model was specified by Wilkinson's notation $RSFA_{LV} \sim 1 + COVID\text{-}19\ Severity_{LV} + CRD_{PC1} + CRD_{PC2} + Age + Sex$. The model can therefore identify unique variance explained by each of the predictors, i.e.,whether COVID-19 $Severity_{LV}$ predicts $RSFA_{LV}$ over and above other predictors. Common effects of interest were the cardiorespiratory-related effects, defined by the common variance between COVID-19 $Severity_{LV}$ and CRD_{PC1} and CRD_{PC2}. Significant effects were identified by nonparametric testing using 10,000 permutations using commonality analysis implementation in Matlab (Wu et al., 2023).

2.5.2.4. COVID-19-related cerebrovascular impairment associations with physical, cognitive, and mental dysfunction. COVID-19-related abnormalities in RSFA identified in the first-level analysis, were related to the two principal components of physical, cognitive, and mental functioning (PCM_{PC1} and PCM_{PC2}) using robust regression. The PCM components were defined as dependent variables in separate models. $RSFA_{LV}$, age and sex were entered as predictors. The model formulas were specified by Wilkinson's notation, '$PCM \sim 1 + RSFA_{LV} + age + sex$' and fitted for the two PCM components separately. To confirm the validity of the results for the significant models, a univariate voxel-wise analyses was performed.

2.5.2.5. Spatial covariance of COVID-19-related cerebrovascular impairment with regional neurotransmitter, metabolic and cell-type distribution. We further assessed the spatial overlap between COVID-19-related cerebrovascular burden map and a range of brain metabolic, neurotransmitter, gene expression and cell-type parameters, including i) existing receptor/metabolic templates and ii) gene transcription profiling maps. Templates of interest included metabolic rates of glucose, oxygen, and aerobic glycolysis (Vaishnavi et al., 2010) and receptor and transmitter maps across nine different neurotransmitter systems (Hansen et al., 2021b), all measured by positron emission tomography (PET). Gene expression maps (Hawrylycz et al., 2012) were based on key proteins implicated in SARS-Cov-2 cellular attachment (angiotensin converting

enzyme-2, ACE2; neuropilin-1, NRP1; neuropilin-2, NRP2), proteolytic processing (cathepsin-B, CTSB; cathepsin-L, CTSL) and viral defence (interferon type 2 receptors, IFNAR2; lymphocyte antigen 6-family member E, LY6E) (Iadecola et al., 2020; Yang et al., 2021). Spatial correlations were evaluated using 10,000 spin-based permutation tests (p-spin) preserving spatial autocorrelation (Alexander-Bloch et al., 2018; Fulcher et al., 2021).

Spatial covariance between the cerebrovascular burden map and gene expression across 9394 genes expressed in the human brain (Hawrylycz et al., 2012) was based on PLS association using spin-premutation-based 10-fold cross-validations (Tsvetanov et al., 2021a). The latent variable represented a spatial pattern of gene expression that covaried significantly with the cerebrovascular burden pattern associated with COVID-19 severity. Full details about the processed transcriptomic data are available elsewhere (Arnatkevičiūtė et al., 2019). Genes highly expressing this pattern (i.e. high loadings) were tested against a molecular atlas of human brain vasculature of 17 control and Alzheimer's disease patients (Yang et al., 2021) using cell-type decomposition (Hansen et al., 2021). This enabled us to test whether the cerebrovascular burden-relevant genes were preferentially expressed in specific cell types, i.e., testing for gene sets specific to eleven major canonical cortical cell classes: astrocytes (Astro); brain endothelial cells (BEC); ependymal cells (Epend); macrophage/microglia (MacMic); meningeal fibroblasts (MFibro); neurons (Neuro); oligodendrocyte precursors (Opc); oligodendrocytes (Oligo); pericytes (*Peri*); perivascular fibroblasts (PFibro); and smooth muscle cells (SMC). To this end, we calculated the ratio of genes in each set preferentially expressed by each cell type (e.g. ratio for pericytes is calculated from the number of genes preferentially expressed in pericytes divided by the total number of genes). Gene sets were thresholded to include the top n% of genes with greatest loadings, where n varied from 10 % to 100 % (all genes). Statistical significance was determined using a null distribution of ratios based on 10,000 sets of random genes (Hansen et al., 2021).

2.6. Data availability and code

Code and composite data to reproduce manuscript figures and statistical analyses are available at https://github.com/kamentsvetanov/covid19_cerebrovascularburden. Resting-state fMRI data were pre-processed using SPM12 and post-processed using a GLM-like approach (Geerligs et al., 2017) available at https://github.com/MRC-CBU/riksneurotools/blob/master/GLM/. MATLAB-based commonality analysis for neuroimaging (Wu et al., 2021) is available at https://github.com/kamentsvetanov/CommonalityAnalysis/. Visualisation of neuroimaging results was in MRIcroGL and BrainSpace. Neurotransmitter receptor and transporter maps were available at https://github.com/netneurolab/hansen_receptors. Spin permutations used code available at https://github.com/frantisekvasa/rotate_parcellation. Fully-preprocessed transcriptomic data were available at https://figshare.com/articles/dataset/AHBAdata/6852911 and https://github.com/BMHLab/AHBAprocessing. The molecular atlas of the human brain vasculature was available at https://www.biorxiv.org/content/https://doi.org/10.1101/2021.04.26.441262v1. Code for cell-type decomposition analysis was available at https://github.com/netneurolab/hansen_genescognition.

3. Results

3.1. Participants

Characteristics of the 45 cases hospitalized with COVID-19 are detailed in Table 1. At hospitalisation, 30 % of the patients required mechanical ventilation (n = 13) for an average of 20 days; 22 % of patients required vasopressors (n = 10), and 9 % required renal replacement therapy with continuous veno-venous haemodiafiltration (n = 4). Most common pre-existing comorbidities at admission with

Covid-19 were cardiovascular dysfunction (n = 11, 24.4 %; hypertension, n = 10; Von Willbrand disease type 1, n = 1), respiratory disorders (n = 8, 17.8 %), type-2 diabetes (n = 4, 8.9 %), hypothyroidism (n = 4, 8.9 %), migraine (n = 2, 4,4%). Other single case conditions included obesity, type-1 diabetes, rheumatoid arthritis, dyslipidaemia, De Quervain's thyroiditis, ulcerative colitis, prostatic arthritis, acute lymphoblastic leukaemia, osteoarthritis, hysterectomy, appendicectomy, acute kidney disease, and non-alcoholic fatty liver disease. The average number of days from initial symptoms to clinical out-patient and research assessments was 169 ± 35 and 180 ± 58, respectively. The percentage of missing values across the inpatient, clinical visit and research visit variables varied between 0 and 38 %. In total 69 out of 405 records (17 %) were incomplete for impatient data; 71 out of 360 records (20 %) were incomplete for clinical visit data; and 121 out of 675 records (18 %) were incomplete for cognitive and mental health data.

3.2. Group differences in cerebrovascular components

The decomposition of RSFA with source-based cerebrovasculometry resulted in 10 spatially independent components according to the MDL criterion with near perfect stability indices across 128 ICASSO iterations (mean of 0.97 and standard deviation of 0.01). One component showed significant difference between the patient and control groups in terms of their subject scores (RSFA$_{IC4}$, t = 3.12, p = 0.003, Fig. 2), while controlling for age and sex in a robust linear regression. The spatial map of this component, labelled RSFA$_{IC4}$, included voxels with high values in temporo-parietal regions, indicating that individuals with higher loading values, in this case the patient group, had lower RSFA values in these regions, relative to the control group (Fig. 2). The other components did not differentiate patients from controls.

The spatial pattern of RSFA$_{IC4}$ was consistent with the univariate voxel-wise approach (r = 0.46, p < 0.001, Fig. 3A). In addition, the univariate approach revealed that the spatial pattern in RSFA associated with age was highly consistent with the one reported on large-scale population-based cohorts, r = 0.42, p < 0.001 (Tsvetanov et al., 2021b; Tsvetanov et al., 2015). This suggests that RSFA can detect reliably differences in cerebrovascular health across various phenotypes in smaller samples. Though age is a risk factor for COVID-19 severity (Verity et al., 2020) and RSFA (Tsvetanov et al., 2021b; Tsvetanov et al., 2015), the COVID-19 group effect was not explained by individual's age, and showed only a partial overlap with the effects of age on RSFA in parietal regions (Fig. 3B) (Tsvetanov et al., 2021b; Tsvetanov et al., 2015).

3.3. COVID-19 severity predicts cerebrovascular impairment

Using PLS analysis, we identified one significant pair of latent variables (r = 0.595, p = 0.011, based on a null distribution of 10,000 permutations). Variable loadings and subject scores reflecting the strong relationship between acute COVID-19 Severity and chronic RSFA abnormalities are shown in Fig. 4.

The RSFA latent variable (RSFA$_{LV}$) expressed negative loadings in frontal (superior frontal gyrus, middle frontal gyrus, inferior frontal gyrus and portions of the anterior cingulate) and parieto-temporal (angular gyrus, supramarginal gyrus, superior temporal gurus, middle temporal gyrus) regions. This pattern of COVID-19 Severity-related reduction in RSFA values was mirrored in a voxel-wise analysis of RSFA maps and the only significant COVID-19 Severity component (p < 0.001) in the inpatient data (Fig. 3C and Fig. 5A, respectively). Positive loadings in the RSFA data appeared to be in postcentral gyrus, calcarine sulcus, cuneus, and lingual gyrus. Increase in the RSFA signal in these regions may reflect increased pulsatility in neighbouring vascular and white matter territories as reported previously (Makedonov et al., 2016; Makedonov et al., 2013b; Tsvetanov et al., 2021b; Tsvetanov et al., 2015). This pair of latent variables suggested that patients with higher COVID-19 Severity at the acute stage have sustained changes in
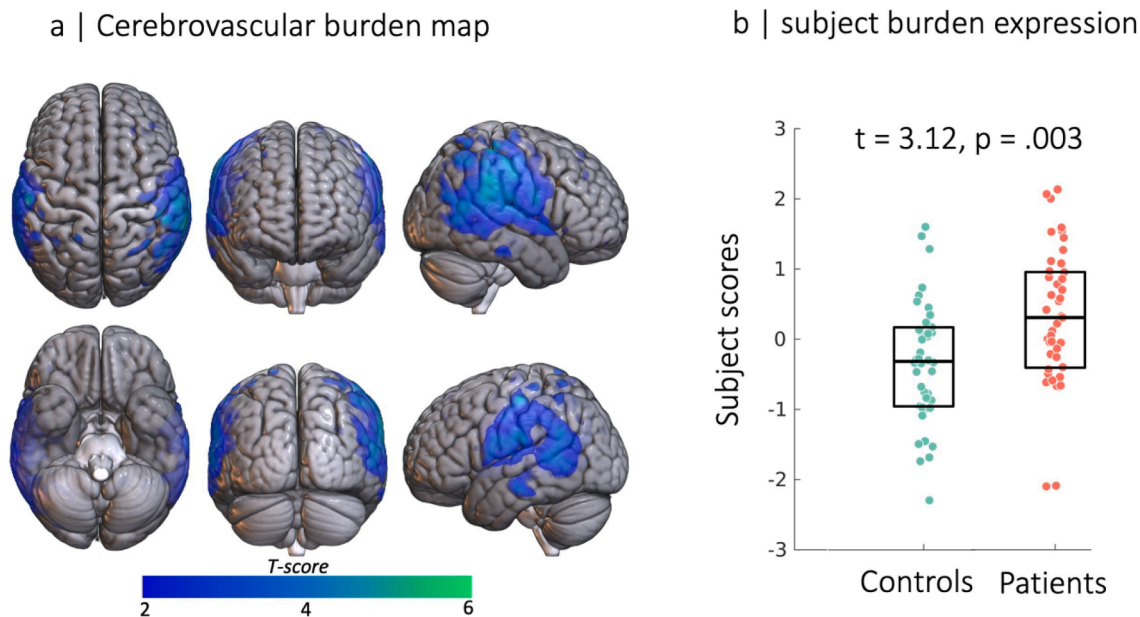
a | Cerebrovascular burden map

b | subject burden expression

Fig. 2. Group differences in RSFA. Source-based cerebrovasculometry for the component differentially expressed between groups: (**a**) independent component spatial map reflecting decrease in RSFA values in temporo-parietal regions. (**b**) Box plots of subject scores for patients hospitalised for COVID-19 (red) and control group (green, each circle represents an individual) indicating higher loading values for patients than controls as informed by two-sample unpaired permutation test (a robust regression was used to down-weight the effects of extreme data points). (For interpretation of the references to colour in this figure legend, the reader is referred to the web version of this article.)

cerebrovascular function in frontal and temporo-parietal regions after discharge from hospital. For visualisation purposes we inverted the loading values in Fig. 4A so that higher values reflect poorer cerebrovascular function, i.e. higher cerebrovascular burden.

To understand whether the relationship between regional RSFA impairment and COVID-19 Severity can be explained by the components of chronic systemic cardiorespiratory dysfunction or covariates of no interest, we performed a second level robust regression analysis. Cardiorespiratory dysfunction was represented by two significant components ($p < 0.001$ and $p < 0.001$; Fig. 5C and D). The first component, CRD_{PC1}, represented overall cardiorespiratory dysfunction in terms of poor lung function, poor oxygen saturation coupled with high pulse pressure. The second component, CRD_{PC2}, represented a more specific component of cardiorespiratory dysfunction in terms of oxygen desaturation and orthostatic hypotension. CRD_{PC2} likely reflects patient differences in sympathetic failure, which is associated with orthostatic fall in blood pressure and oxygenation (Jakobsen et al., 2017). Overall, the two CRD components are consistent with the idea of cardiovascular health being multifactorial, where autonomic nervous system response is clearly dissociated from the two components of blood pressure (King et al., 2022; Tsvetanov et al., 2021b). The regression model specification was based on the following syntax using Wilkinson notation: $RSFA_{LV} \sim 1 + COVID\text{-}19Severity_{LV} + CRD_{PCA1} + CRD_{PCA2} + Age + Sex$. COVID-19 Severity was the only significant predictor of $RSFA_{LV}$ in the model ($r = 0.490$, $p < 0.001$), suggesting that chronic cardiorespiratory dysfunction, age and sex cannot explain fully the relationship between COVID-19 Severity and RSFA abnormality. None of the pre-existing comorbidity conditions explained this relationship (e.g. by adding co-morbidity categories as covariates of no interest, COVID-19 Severity remained highliy significant predictor, $r = 0.451$, $p < 0.001$; noting that having a respiratory condition was independently associated with $RSFA_{LV}$, $r = 0.336$, $p = 0.004$). Interestingly, the unique variance explained by COVID-19 Severity in the regression model was weaker than the variance identified by the PLS analysis ($r = 0.595$ vs $r = 0.490$ for PLS and MLR analyses) suggesting that one or more of the predictors in the model explain some of the covariance between COVID-19 Severity and RSFA. Permutation-based commonality analysis with 10,000

permutations confirmed that a portion of the variance between COVID-19 Severity$_{LV}$ and RSFA$_{LV}$ was explained uniquely by age (13 % total, $p < 0.001$) or cardiorespiratory dysfunction component 2 (CRD_{PC2}, 4 % total, $p = 0.002$), or by shared effects of age and cardiorespiratory dysfunction component 1 (Age, CRD_{PC1}, 18 % total, $p < 0.001$), SI Table 1. COVID-19 Severity$_{LV}$ remained as the largest unique predictor of variance in RSFA$_{LV}$ (40 % total, $p = 0.004$).

3.4. COVID-19-related cerebrovascular burden association with physical, cognitive, and mental functioning

The level of RSFA abnormalities (RSFA$_{LV}$) was related to physical, cognitive and mental dysfunction represented by two significant components ($p < 0.001$ and $p < 0.001$). The first component, PCM_{PC1}, expressed highly mental health variables (GAD-7, PCL-5, PHQ-9, PHQ-15 and SF-36 sub-scores), thus reflecting overall mental health (PCM_{PC1}, Fig. 5E). The second component, PCM_{PC2}, expressed highly cognitive function and functional independence variables (Barthel Index, MoCA and iMRS, Fig. 5F). RSFA$_{LV}$, age and sex were entered as predictors, while PCM components were used as dependent variables in separate robust regression model (Model 1: $PCM_{PCA1} \sim 1 + RSFA_{LV} + age + sex$; Model 2: $PCM_{PCA2} \sim 1 + RSFA_{LV} + age + sex$). Model 1 was not significant ($p = 0.447$), while Model 2 was significant ($R2 = 0.303$, $p = 0.002$) with RSFA significantly related to PCM_{PC2} ($r = -0.362$, $p = 0.010$). This indicates that patients with higher RSFA abnormality have worse cognitive function and less functional independence. None of the pre-existing comorbidity conditions explained this relationship (e.g. by adding comorbidity categories as covariates of no interest), RSFA remained significant predictor of PCM_{PC2}, $r = -0.550$, $p = 0.001$. The findings in Model 2 were confirmed using voxel-wise analysis on RSFA maps, instead of RSFA$_{LV}$ (Fig. 3D).

3.5. Spatial overlap of COVID-19-related cerebrovascular impairment with brain neurotransmitter and metabolic distribution

We next assessed the spatial overlap between COVID-19-related cerebrovascular burden maps with existing neurotransmitter and
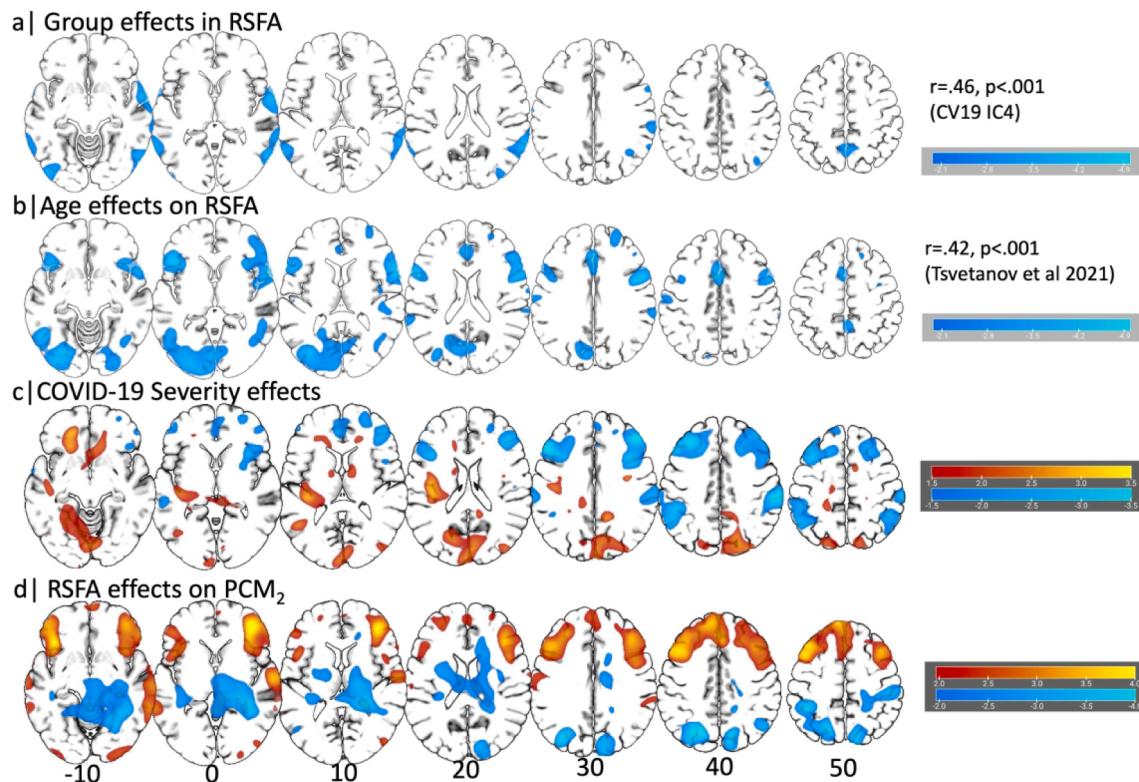
Fig. 3. Voxel-wise association in RSFA data. Association between RSFA and group identity (patient vs control) **(a)** To confirm the validity of results from the source-based cerebrovasculometry, we performed a second-level univariate analysis in SPM12 with RSFA as dependent variable. Group identity, age and sex were defined as predictors. The spatial pattern of group effects was highly consistent with the pattern identified using ICA (IC4), r = 0.46, p-spin < 0.001. **(b)** The spatial pattern associated with age effect was highly consistent with the pattern derived from a previous study using a large population-based cohort (n = 226, Tsvetanov et al., 2021b), r = 0.42, p-spin < 0.001. **(c)** Association between COVID-19 Severity PC1 (see Fig. 5A) and RSFA on voxel level showing a negative association between COVID-19 Severity and RSFA values in frontal and temporoparietal regions confirming the validity of the results in the partial-least squares analysis capturing the multivariate relationship between COVID-19 severity and cerebrovascular impairment. This was based on a second-level univariate analysis in SPM12 with RSFA as dependent variable. COVID-19 severity component, age and sex were defined as predictors. The nine measures constructing the COVID-19 severity component (COVID-19 Severity$_{PC1}$) included COVID-19 WHO Progression Scale and blood markers (CRP, ferritin, IL-6, bilirubin, D-dimer, PT, APTT and iPlatelets), see Fig. 5A. The model can be represented using Wilkinson's notation as follows: *RSFA ~ 1 + COVID-19 Severity$_{PC1}$ + Age + Sex.* **(d)** Association between the second physical, cognitive, and mental functioning component (PCM$_{PC2}$) and RSFA on voxel level showing a positive association between phsyical and cognitive functioning with RSFA values in frontal and temporall regions. Maps are thresholded at uncorrected p-values of 0.05 for more complete description of the spatial representation.
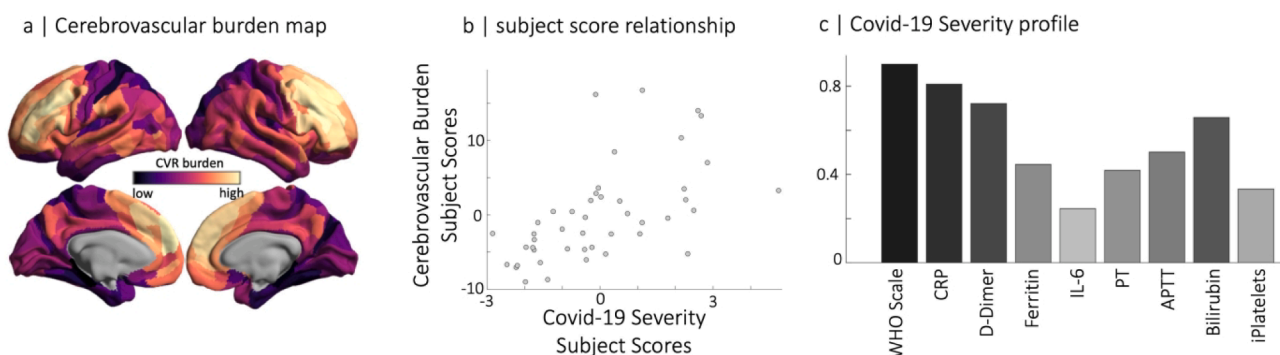

Fig. 4. Link between COVID-19 severity and RSFA. Partial least squares analysis of COVID-19 severity data at acute stage and RSFA-based cerebrovascular burden (CVB) at chronic stage. (**a**) Spatial distribution of parcellated RSFA values where dark to light colours are used for the strength of positive and negative correlations with the COVID-19 Severity profile (**c**). Note that regions with high cerebrovascular burden have low values in RSFA. (**b**) The scatter plot in the middle panel represents the relationship between subjects scores of RSFA-latent variable and COVID-19 Severity-latent variable identified by partial least squares analysis.

metabolic maps using spatial autocorrelation-preserving permutation testing (Alexander-Bloch et al., 2018). Across 21 candidate maps, we show that the cerebrovascular burden map overlaps with the distribution of serotonin's vasoactive receptor 5-HT1b (r = 0.52, p-spin < 0.001), aerobic glycolysis (r = 0.51, p-spin < 0.001) and to a weaker extent cerebral metabolic rate of glucose in the brain (r = 0.38, p-spin$_{one-}$

$_{sided}$ = 0.041). However, the regional distribution of RSFA abnormality showed little correlation with the expression of key proteins implicated in SARS-CoV-2 cellular attachment, processing and viral defence (Fig. 6). Collectively, these results demonstrate that the distribution of cerebrovascular impairment related to COVID-19 severity is aligned with the spatial distribution of receptors and processes involved in the
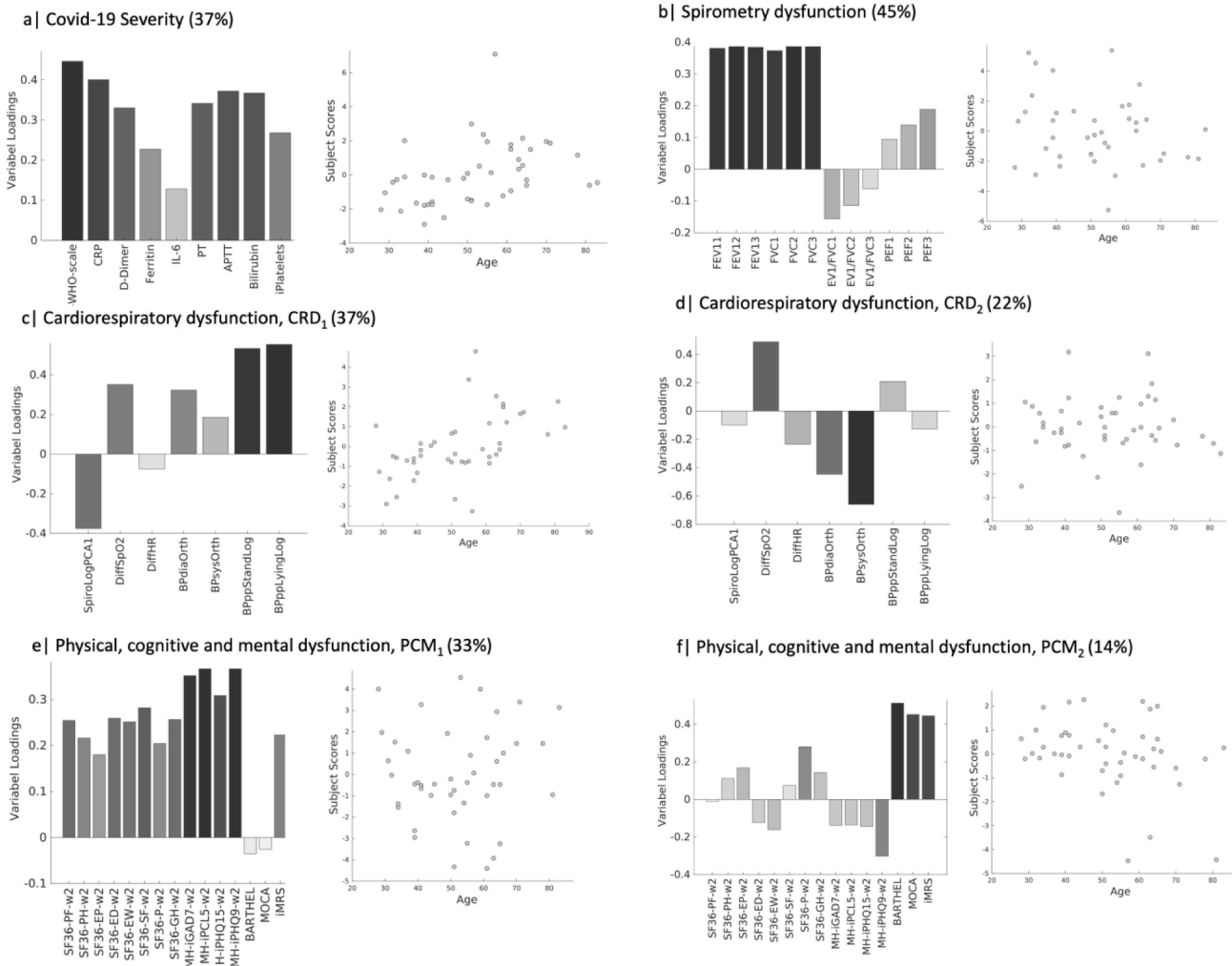
Fig. 5. Data reduction of inpatient, clinical and research visit non-neuroimaging data using principal component analysis (separately on each dataset). **(a)** COVID-19 Severity component explaining 40% of the total variance loading most strongly on WHO COVID-19 11-point Progression scale (WHO-scale), C-reactive protein (CRP), D-dimer, ferritin, followed by bilirubin and activated partial thromboplastin time (APTT). Other biomarkers [interleukin-6, prothrombin time (PT), platelets (iPlatelets, counts so that higher scores represent lower counts)] loaded in the expected direction, but to a lesser extent. Scatter plots of subject scores for the corresponding components versus chronological age, where each circle is one patient. **(b)** Reduction of spirometry measures to a single variable to balance the representativeness of each data type for cardiorespiratory dysfunction dimensionality reduction (Hastie et al., 2009). Of the 12 spirometry measures the first principal component expressed FEV1 and FVC values explaining 45% of the spirometry data. FEV1 – forced expiratory volume in 1 s; PEF – peak expiratory flow; FVC – forced vital capacity. **(c)** First cardiorespiratory dysfunction component (CRD$_1$) constructed from chronic cardiorespiratory data, explaining 37% and loading highly on lung function, oxygen saturation and pulse pressure. **(d)** The second component, explaining 22%, loaded on oxygen saturation and orthostatic hypotension. SpiroLogPCA1 – first principal component across 12 log-transformed spirometry variables (see panel **b**); DiffSpO2 and DiffHR – difference in arterial oxygen saturation and heart rate before and after a 6-minute walk test; BPdiaOrth and BPsysOrth – orthostatic intolerance in diastolic and systolic blood pressure, respectively; BPppStandLog and BPppLyingLog – pulse pressure while standing and lying, respectively. **(e)** The first component of physical, cognitive and mental dysfunction (PCM$_1$) explaining 33% and loading highly on mental health variables. **(f)** PCM$_2$ explaining 14% and loading positively on cognitive function and functional independence. SF36-PF – physical functioning; SF36-RLP – role limitation physical, SF36-RLE – role limitation emotional, SF36-ED – energy dimension, SF36-EW – emotional wellbeing, SF36-SF – social functioning, SF-P – pain; SF36-GH – general health; iGAD7 – Generalised Anxiety Disorder-7; PCL5 – Posttraumatic Stress Disorder Checklist-5; PHQ15 – Patient Health Questionnaire-15; PHQ9 – Patient Health Questionnaire-9; BARTHEL – Barthel Index; MOCA – Montreal Cognitive Assesment; iMRS – inverted Modified Ranking Scale;

coordination of metabolic and vasoreactive responses.

As a final step, we used normative transcriptomics to identify genes that are normally preferentially expressed in the regions associated with COVID-19-induced cerebrovascular impairment. Regularised-PLS identified one latent component (r = 0.64, p = 0.001, Fig. 7A). Using cell-type decomposition analysis on vascular cell-type specific gene sets, we determined the ratio of genes in each gene set preferentially expressed across eleven cortical cell types. Gene-sets were thresholded to include the top 70 % of genes with the highest loadings (Fig. 7B). While the 70 % threshold was arbitrary, that results were consistent across thresholds ranging from 10 to no threshold. Highly ranking genes

were significantly more expressed in pericytes, brain endothelial cells and neurons, and significantly less expressed in oligodendrocytes. Broadly, we find evidence that areas associated with cerebrovascular impairment are enriched for expression of genes related to neuron support (pericytes, endothelial cells and perineuronal oligodendrocytes) and neurons themselves. This dichotomy is consistent with the observations from the spatial overlap analysis i.e. cerebrovascular impairment spatially covaries with expression of genes, receptors and processes involved in the coordination of metabolic and vasoreactive responses essential for neuronal homeostasis.
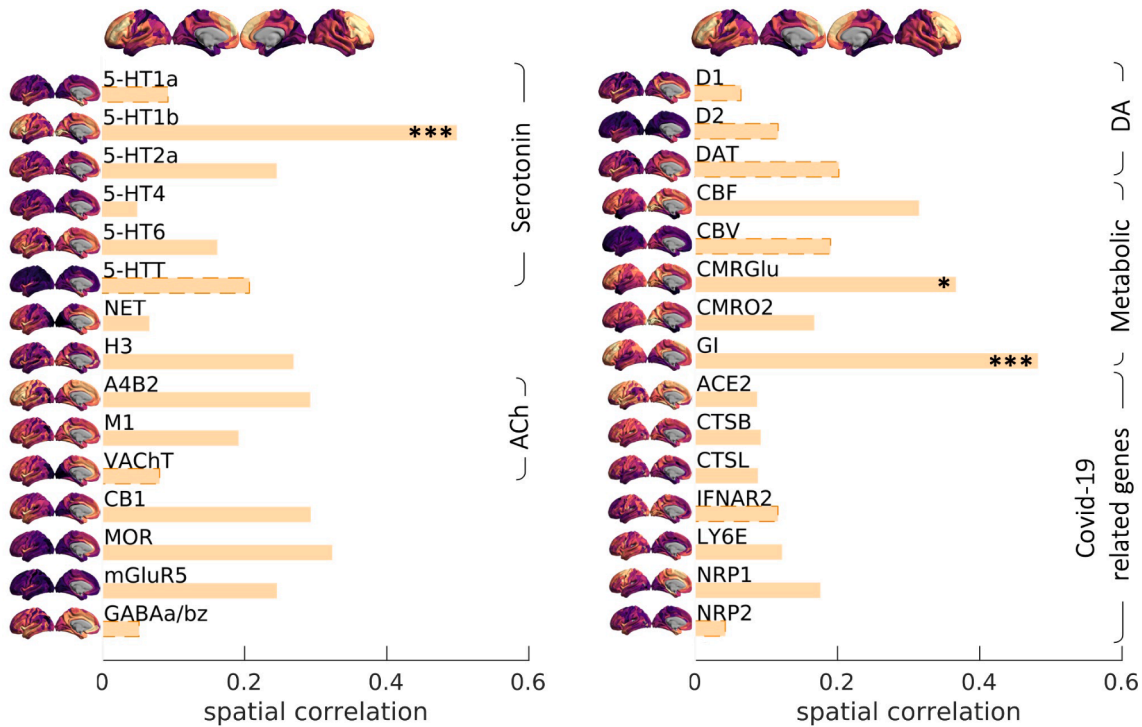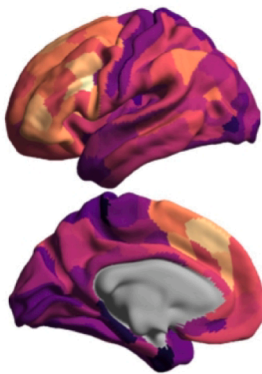
Fig. 6. Spatial correspondence between COVID-19-related cerebrovascular burden map with neurotransmitter and brain distributions. Spatial correlation between Covid19 severity-induced cerebrovascular burden map and spatial patterns associated with a range of neurotransmitter receptor/transporters (Hansen et al., 2021b), selected genes relevant to SARS-CoV-2 brain entry (Iadecola et al., 2020) and brain metabolism parameters (Vaishnavi et al., 2010). Neurotransmitter receptors and transporters were selective to serotonin (5-HT1a, 5-HT1b, 5-HT2a, 5-HT4, 5-HT6, 5-HTT), norepinephrine (NET), histamine (H3), acetylcholine (ACh, A4B2, M1, VAChT), cannabinoid (CB1), opioid (MOR), glutamate (mGluR5), GABA (GABAa/bz) and dopamine (D1, D2, DAT). Metabolic maps were based on cerebral blood flow (CBF), cerebral blood volume (CBV), cerebral metabolic rate of glucose and oxygen (CMRGlu, CMRO2) and glycemic index (GI). Selective genes relevant to SARS-CoV-2 brain entry included angiotensin converting enzyme-2, ACE2; neuropilin-1, NRP1; neuropilin-2, NRP2, cathepsin-B, CTSB; cathepsin-L, CTSL, interferon type 2 receptors, IFNAR2; lymphocyte antigen 6-family member E, LY6E. The spatial maps of 5-HT1b, CMRGlu and Glycemic Index (GI) were significantly correlated with Covid19 severity-induced cerebrovascular burden map (* p-spin < 0.05 (one-sided), *** p-spin < 0.001). See text for more information.
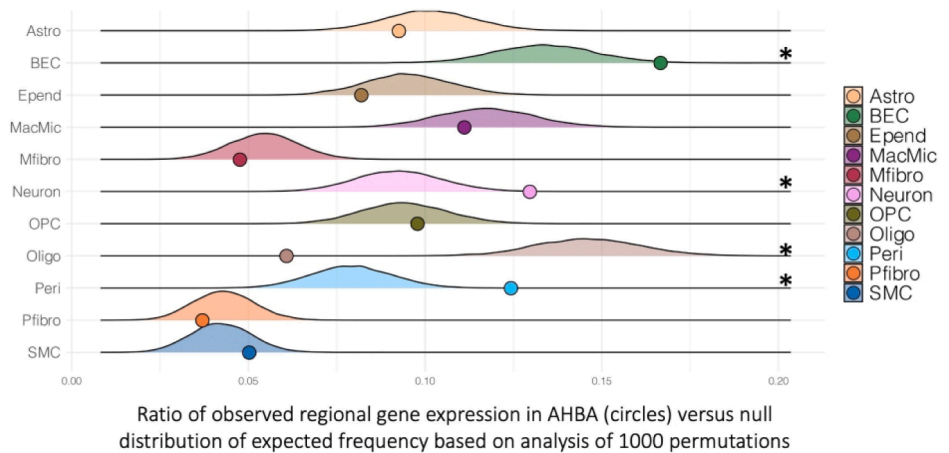

Fig. 7. Spatial correspondence between COVID-19-related cerebrovascular burden and cell-type decomposition. (**a**) Spatial map of the weighted whole genome expression profile correlated with the COVID-19-induced cerebrovascular burden map (CVB). (**b**) Cell-type decomposition was used to identify cell-type enrichment based on extent to which genes expressed the transcriptome map in a. Gene sets for each cell-type was constructed by thresholding the top 70 % of genes with greatest loadings. Note that results were consistent across a range of thresholds, ranging from 10 % to no threshold. The ratio of genes in each gene set preferentially expressed in eleven distinct cell-types (circles) is shown against their null distribution of a model with random selection of all genes (10,000 permutations, *p-value < 0.05). For example, pericyte's ratio is calculated from the number of genes preferentially expressed in pericytes divided by the total number of genes. Cell type-specificity of genes is described elsewhere (Yang et al., 2021) Astro – astrocytes, BEC – brain endothelial cells, Epend – ependymal, MacMic – macrophage/microglia, Mfibro – meningeal fibroblast, Neuron – neuron, OPC – oligodendrocyte precursor cells, Oligo – oligodendrocytes, *Peri* – pericytes, Pfibro – perivascular fibroblast, SMC – smooth muscle cells.

4. Discussion

We show that abnormalities in cerebral microvascular function, measured using resting state fluctuation amplitudes, RSFA, persist many months (on average six months in our sample) after hospitalisation for acute COVID-19. The location of these abnormalities in lateral frontal and temporoparietal regions aligns partly with cerebrovascular dysfunction reported in association with ageing (Tsvetanov et al., 2021b; Tsvetanov et al., 2015) preclinical Alzheimer's disease (Millar et al., 2020a) and systemic cardiovascular health (Tsvetanov et al., 2021b).These post-COVID-19 effects were observed over and above age. These effects are related to severity of the acute illness and the host response in the acute stage. These effects also relate to the post-COVID-19 cognitive function, common indices of mental health, and quality of life at an average of six months after hospitalisation.

In spatial covariance analyses, we found overlap between the regional distribution of this cerebrovascular impairment and spatial distribution of the vasoreactive receptor 5-HT1b and regions with high metabolic demands. 5-HT1b receptor is the dominant contractile 5-HT receptor in cerebral arteries (Barnes and Hoyer, 2021; Nilsson et al., 1999), stimulating vasoconstriction by contracting smooth muscle directly or as a moderator of other vasoconstrictors. Distinct from its effects on vascular tone, the presynaptic 5-HT1b receptor also has an important microvascular anti-inflammatory role, both in the cerebrovascular bed and more generally. Further, its loss has been implicated in progressive cognitive loss and abnormal modulation through descending serotonergic outputs (Gharishvandi et al., 2020; Heijmans et al., 2021; Mitsikostas et al., 2002; Sibille et al., 2007), which may be relevant for chronic sequelae after COVID-19.

The overlap of cerebrovascular impairment with the regional distribution of aerobic glycolysis and glucose metabolism is spatially concordant with previous reports of hypometabolism in the subacute phase of COVID-19 (Hosp et al., 2021) and neurodegeneration (Vlassenko et al., 2010). This indicates a potential link between cerebrovascular impairment and metabolic dysfunction in frontoparietal regions, which could provide important insights regarding the mechanisms of late neurocognitive dysfunction following COVID-19 infection. Future work should establish whether changes to the microvasculature lead to hypometabolism (Shi et al., 2016) or whether the vulnerability of brain physiology in the chronic phase is due to hypoxic and hypometabolic exposure in the subacute phase (Vestergaard et al., 2020). Collectively, these results demonstrate that the distribution of chronic cerebrovascular impairments related to COVID-19 severity maps to the spatial distribution of processes involved in coordinating metabolic and vasoregulatory responses associated with changes in brain function and cognition.

We also tested whether genes highly expressed in regions with COVID-19-induced cerebrovascular change are preferentially expressed in specific cell types using a molecular atlas of human brain vasculature (Yang et al., 2021). Dominant genes were overexpressed in pericytes, brain endothelial cells and neurons, but underexpressed in oligodendrocytes. The evidence that genes implicated are enriched in pericytes and endothelial cells is particularly interesting. Brain endothelial cells are susceptible to direct SARS-CoV-2 infection through flow-dependent expression of ACE2. The SARS-CoV-2 S protein binding triggers a gene expression profile that may compromise the neurovascular interface (Kaneko et al., 2021). On the abluminal aspect of the neurovascular interface, pericytes express abundantly the angiotensin-converting enzyme-2 (ACE2) receptor (He et al., 2020). The expression can be increased by exposure to the viral S protein, and importantly, potentiated in combination with hypoxia (Khaddaj-Mallat et al., 2021), a mechanism that could account for the modulation of RSFA abnormality by disease severity in our cohort.

Given this biological context the correlation of RSFA abnormalities with disease severity is open to two potential interpretations. One possibility is that these changes in cerebrovascular regulatory integrity are the consequence of direct viral invasion; while the other is that these abnormalities are a consequence of the inflammatory host response, which is a consequence of, but may not scale precisely with, viral infection. Spatial correlation of RSFA abnormality with the expression of ACE2 and Neuropilin-1, or of genes involved in cellular responses to viral infection would have provided supportive evidence of a role for direct viral infection as a mechanism, but we were unable to demonstrate such correlations. These negative findings favour the explanation that host inflammatory responses may be drivers in this context, and merit further investigation as mechanisms of late cerebrovascular regulatory dysfunction, consistent with the hypothesis of long COVID endotheliopathy (Ahamed and Laurence, 2022). It is important to acknowledge that our correlations with regional gene expression are based on expression patterns in normal brain, and that these expression patterns may be substantially altered by the inflammatory milieu that prevails in the context of COVID-19. Consequently, direct examination of peripheral blood gene expression profiling in late COVID-19 survivors would provide additional insights.

Our study has several limitations. We are limited (i) by the relatively small sample size with incomplete data across modalities and patients (Jakobsen et al., 2017), (ii) by sensitivity to domain-specific cognitive impairment (Coen et al., 2016) and (iii) by the absence of longitudinal imaging data in patients and physiological data in controls. We also can not draw any causal inferences from the associations we observe. However, the demonstration of functional microvascular abnormalities following COVID-19 is important to understand the potential mechanisms of persistent cognitive and mental health problems. The association of microvascular abnormalities with late outcomes of relevance to patients, and the fact that they represent an easily accessible biomarker, suggest both a potential therapeutic target and/or a biomarker of treatment effect in interventional studies. It remains to be shown whether the localisation of RSFA abnormalities to regions rich in 5HT-1b receptors is a consequence of overactivity of these receptors (resulting in low cerebral blood flow), underactivity or loss of these receptors (resulting in vasoparalysis and/or inflammation), or a manifestation of flow-metabolism mismatching with inadequate substrate and oxygen delivery. This is relevant as potential therapeutic agents are available to modulate both 5HT-1b function (Barnes et al 2021) and inflammatory response (Group and Sterne, 2021; Zhang et al., 2020).

In summary, we demonstrate that the severity of acute COVID-19 predicts cerebrovascular impairment six months later. The cerebrovascular abnormality was associated with worse cognitive function, mental health, functional recovery, and quality of life months after hospitalisation. Localised across lateral frontotemporoparietal regions, we show that the physiological and genetic signature of this cerebrovascular impairment shapes the composition of cell-types, metabolism and vasoreactivity essential for neuronal homeostasis. Collectively, these results implicate long-lasting COVID-19-related vulnerability of brain systems differentially relying on metabolic physiology and cell biology in support of their functional specialisation.

CRediT authorship contribution statement

Kamen A. Tsvetanov: Conceptualization, Methodology, Software, Formal analysis, Visualization, Writing – original draft, Writing – review & editing. **Lennart R.B. Spindler:** Data curation, Writing – review & editing. **Emmanuel A. Stamatakis:** Writing – review & editing. **Virginia F.J. Newcombe:** Investigation, Writing – review & editing. **Victoria C. Lupson:** Investigation, Writing – review & editing. **Doris A. Chatfield:** Data curation, Investigation, Writing – review & editing. **Anne E. Manktelow:** Data curation, Investigation, Writing – review & editing. **Joanne G. Outtrim:** Data curation, Investigation, Writing – review & editing. **Anne Elmer:** Investigation, Writing – review & editing. **Nathalie Kingston:** Investigation, Writing – review & editing. **John R. Bradley:** Investigation, Writing – review & editing. **Edward T. Bullmore:** Conceptualization, Methodology, Funding acquisition,

Project administration, Supervision, Writing – review & editing. **James B. Rowe:** Conceptualization, Methodology, Funding acquisition, Project administration, Supervision, Writing – original draft, Writing – review & editing. **David K. Menon:** Conceptualization, Methodology, Funding acquisition, Project administration, Supervision, Writing – original draft, Writing – review & editing.

Declaration of Competing Interest

The authors declare that they have no known competing financial interests or personal relationships that could have appeared to influence the work reported in this paper.

Data availability

Code and composite data to reproduce manuscript figures and statistical analyses will be made available at https://github.com/kamentsvetanov/covid19_cerebrovascularburden. More detailed data may be available on request, with enquiries directed to dac@bioresource.nihr.ac.uk.

Potential Conflicts of interests

All authors have no conflicts of interest. Untreated to this there are several disclosures.

VFJN holds a grant from Roche Pharmaceuticals on proteomic biomarkers in traumatic brain injury and reports personal fees from Neurodiem.

ETB serves as a consultant for Boehringer Ingelheim, GlaxoSmithKline, Monument Therapeutics and Sosei Heptares.

JBR serves as an associate editor to Brain and is a non-remunerated trustee of the Guarantors of Brain, Darwin College and the PSP Association (UK). He provides consultancy to Asceneuron, Biogen, UCB and

has research grants from AZ-Medimmune, Janssen, and Lilly as industry partners in the Dementias Platform UK.

DKM reports grants, personal fees, and nonfinancial support from GlaxoSmithKline Ltd.; grants, personal fees, and other from Neuro-Trauma Sciences; grants and personal fees from Integra Life Sciences; personal fees from Pfizer Ltd.; grants and personal fees from Lantmannen AB; from Calico Ltd.; personal fees from Pressura Neuro Ltd.; and others from Cortirio Ltd., outside the submitted work.

Appendix A. Supplementary data

Supplementary data to this article can be found online at https://doi.org/10.1016/j.nicl.2022.103253.

References

Agarwal, S., Sair, H., Gujar, S., Hua, J., Lu, H., Pillai, J., 2019. Functional Magnetic Resonance Imaging Activation Optimization in the Setting of Brain Tumor-Induced Neurovascular Uncoupling Using Resting-State Blood Oxygen Level-Dependent Amplitude of Low Frequency Fluctuations. Brain Connect 9, 241–250. https://doi.org/10.1089/BRAIN.2017.0562.

Ahamed, J., Laurence, J., 2022. Long COVID endotheliopathy: hypothesized mechanisms and potential therapeutic approaches. J Clin Invest 132. https://doi.org/10.1172/JCI161167.

Ainslie, P.N., Ashmead, J.C., Ide, K., Morgan, B.J., Poulin, M.J., 2005. Differential responses to CO2 and sympathetic stimulation in the cerebral and femoral circulations in humans. J Physiol 566, 613–624. https://doi.org/10.1113/jphysiol.2005.087320.

Alexander-Bloch, A.F., Shou, H., Liu, S., Satterthwaite, T.D., Glahn, D.C., Shinohara, R.T., Vandekar, S.N., Raznahan, A., 2018. On testing for spatial correspondence between maps of human brain structure and function. Neuroimage 178, 540. https://doi.org/10.1016/J.NEUROIMAGE.2018.05.070.

Arnatkevičiūtė, A., Fulcher, B.D., Fornito, A., 2019. A practical guide to linking brain-wide gene expression and neuroimaging data. Neuroimage 189, 353–367.

Asakura, H., Ogawa, H., 2021. COVID-19-associated coagulopathy and disseminated intravascular coagulation. Int J Hematol 113 (1), 45–57.

Bangash, M.N., Patel, J., Parekh, D., 2020. COVID-19 and the liver: little cause for concern. Lancet Gastroenterol Hepatol 5, 529–530. https://doi.org/10.1016/S2468-1253(20)30084-4.

Barnes, N.M., Hoyer, D., 2021. International Union of Basic and Clinical Pharmacology. CX. Classification of Receptors for 5-hydroxytryptamine; Pharmacology and Function. Pharmacol Rev 73 (1), 310–520.

Barnes, N.M., Ahern, G.P., Becamel, C., Bockaert, J., Camilleri, M., Chaumont-Dubel, S., Claeysen, S., Cunningham, K.A., Fone, K.C., Gershon, M., Di Giovanni, G., Goodfellow, N.M., Halberstadt, A.L., Hartley, R.M., Hassaine, G., Herrick-Davis, K., Hovius, R., Lacivita, E., Lambe, E.K., Leopoldo, M., Levy, F.O., Lummis, S.C.R., Marin, P., Maroteaux, L., McCreary, A.C., Nelson, D.L., Neumaier, J.F., Newman-Tancredi, A., Nury, H., Roberts, A., Roth, B.L., Roumier, A., Sanger, G.J., Teitler, M., Sharp, T., Villalón, C.M., Vogel, H., Watts, S.W., Hoyer, D., Ohlstein, E.H., 2021. International Union of Basic and Clinical Pharmacology. CX. Classification of Receptors for 5-hydroxytryptamine; Pharmacology and Function. Pharmacol Rev 73 (1), 310–520.

Birn, R.M., Diamond, J.B., Smith, M.a., Bandettini, P.a., 2006. Separating respiratory-variation-related fluctuations from neuronal-activity-related fluctuations in fMRI. Neuroimage 31, 1536–1548. https://doi.org/10.1016/j.neuroimage.2006.02.048.

Blevins, C.A., Weathers, F.W., Davis, M.T., Witte, T.K., Domino, J.L., 2015. The Posttraumatic Stress Disorder Checklist for DSM-5 (PCL-5): Development and Initial Psychometric Evaluation. J Trauma Stress 28, 489–498. https://doi.org/10.1002/JTS.22059.

Brandes, R., Fleming, I., Busse, R., 2005. Endothelial aging. Cardiovasc Res 66 (2), 286–294.

Calhoun, V., Adali, T., Pearlson, G., Pekar, J., 2001. A method for making group inferences from functional MRI data using independent component analysis. Hum Brain Mapp 14, 140–151. https://doi.org/10.1002/hbm.

Chen, X., Laurent, S., Onur, O.A., Kleineberg, N.N., Fink, G.R., Schweitzer, F., Warnke, C., 2021. A systematic review of neurological symptoms and complications of COVID-19. J Neurol 268 (2), 392–402.

Coen, R.F., Robertson, D.A., Kenny, R.A., King-Kallimanis, B.L., 2016. Strengths and Limitations of the MoCA for Assessing Cognitive Functioning: Findings From a Large Representative Sample of Irish Older Adults. J Geriatr Psychiatry Neurol 29, 18–24. https://doi.org/10.1177/0891988715598236.

R.O. Crapo R. Casaburi A.L. Coates P.L. Enright N.R. MacIntyre R.T. McKay D. Johnson J. S. Wanger R.J. Zeballos V. Bittner C. Mottram ATS Statement: Guidelines for the six-minute walk test. 2012 10.1164/ajrccm.166.1.at1102 166, 111-117. https://doi.org/10.1164/AJRCCM.166.1.AT1102.

E. Dobriban Permutation methods for factor analysis and PCA Permutation methods for factor analysis and PCA. 48 5 2020 10.1214/19-AOS1907 48, 2824-2847. https://doi.org/10.1214/19-AOS1907.

R.M. du Bois D. Weycker C. Albera W.Z. Bradford U. Costabel A. Kartashov L. Lancaster P.W. Noble S.A. Sahn J. Szwarcberg M. Thomeer D. Valeyre T.E. King, Jr. Six-

Minute-Walk Test in Idiopathic Pulmonary Fibrosis. 183 2012 1231 1237 10.1164/rccm.201007-1179OC https://doi.org/10.1164/RCCM.201007-1179OC.

Enright, P.L., McBurnie, M.A., Bittner, V., Tracy, R.P., McNamara, R., Arnold, A., Newman, A.B., 2003. The 6-min walk test: a quick measure of functional status in elderly adults. Chest 123, 387–398. https://doi.org/10.1378/CHEST.123.2.387.

Eriksson, M., Appelros, P., Norrving, B., Terént, A., Stegmayr, B., 2007. Assessment of Functional Outcome in a National Quality Register for Acute Stroke. Stroke 38, 1384–1386. https://doi.org/10.1161/01.STR.0000260102.97954.9C.

Fulcher, B.D., Arnatkeviciute, A., Fornito, A., 2021. Overcoming false-positive gene-category enrichment in the analysis of spatially resolved transcriptomic brain atlas data. Nat Commun 12 (1).

Gao, Y.-Z., Zhang, J.-J., Liu, H., Wu, G.-Y., Xiong, Li., Shu, M., 2013. Regional cerebral blood flow and cerebrovascular reactivity in Alzheimer's disease and vascular dementia assessed by arterial spinlabeling magnetic resonance imaging. Curr Neurovasc Res 10 (1), 49–53.

Geerligs, L., Tsvetanov, K.A., Cam-CAN, Henson, R.N., 2017. Challenges in measuring individual differences in functional connectivity using fMRI: The case of healthy aging. Hum Brain Mapp 38 (8), 4125–4156.

Gharishvand, F., Abdollahi, A., Shafaroodi, H., Mohammad Jafari, R., Pasalar, P., Dehpour, A., 2020. Involvement of 5-HT1B/1D receptors in the inflammatory response and oxidative stress in intestinal ischemia/reperfusion in rats. Eur J Pharmacol 882, 173265.

Glasser, M.F., Coalson, T.S., Robinson, E.C., Hacker, C.D., Harwell, J., Yacoub, E., Ugurbil, K., Andersson, J., Beckmann, C.F., Jenkinson, M., Smith, S.M., Van Essen, D. C., 2016. A multi-modal parcellation of human cerebral cortex. Nature 536 (7615), 171–178.

Glover, G.H., Shmueli, K., van Gelderen, P., de Zwart, J.A., Horovitz, S.G., Fukunaga, M., Jansma, J.M., Duyn, J.H., 2007. Low-frequency fluctuations in the cardiac rate as a source of variance in the resting-state fMRI BOLD signal. Neuroimage 38 (2), 306–320. https://doi.org/10.1016/j.neuroimage.2007.07.037.

Golestani, A.M., Wei, L.L., Chen, J.J., 2016. Quantitative mapping of cerebrovascular reactivity using resting-state BOLD fMRI: Validation in healthy adults. Neuroimage 138, 147–163. https://doi.org/10.1016/j.neuroimage.2016.05.025.

Group, T. W. H. O. R. E. A. for C.-19 T. (REACT) W., Sterne, J.A.C, 2021. Association Between Administration of IL-6 Antagonists and Mortality Among Patients Hospitalized for COVID-19: A Meta-analysis. JAMA 326 (6), 499–518. https://doi.org/10.1001/JAMA.2021.11330.

Hanafi, R., Roger, P.-A., Perin, B., Kuchcinski, G., Deleval, N., Dallery, F., Michel, D., Hacein-Bey, L., Pruvo, J.-P., Outteryck, O., Constans, J.-M., 2020. COVID-19 Neurologic Complication with CNS Vasculitis-Like Pattern. American Journal of Neuroradiology 41, 1384–1387. https://doi.org/10.3174/AJNR.A6651.

Hansen, J.Y., Shafiei, G., Markello, R.D., Smart, K., Cox, S.M.L., Wu, Y., Gallezot, J.-D., Aumont, É., Servaes, S., Scala, S.G., DuBois, J.M., Wainstein, G., Bezgin, G., Funck, T., Schmitz, T.W., Spreng, R.N., Soucy, J.-P., Baillet, S., Guimond, S., Hietala, J., Bédard, M.-A., Leyton, M., Kobayashi, E., Rosa-Neto, P., Palomero-Gallagher, N., Shine, J.M., Carson, R.E., Tuominen, L., Dagher, A., Misic, B., 2021b. Mapping neurotransmitter systems to the structural and functional organization of the human neocortex. bioRxiv 2021.10.28.466336. https://doi.org/10.1101/2021.10.28.466336.

Hansen, J.Y., Markello, R.D., Vogel, J.W., Seidlitz, J., Bzdok, D., Misic, B., 2021. Mapping gene transcription and neurocognition across human neocortex. Nat Hum Behav 5 (9), 1240–1250.

T. Hastie R. Tibshirani J. Friedman Model Assessment and Selection 2009 10.1007/978-0-387-84858-7_7 219 259.

Hawrylycz, M.J., Lein, E.S., Guillozet-Bongaarts, A.L., Shen, E.H., Ng, L., Miller, J.A., van de Lagemaat, L.N., Smith, K.A., Ebbert, A., Riley, Z.L., Abajian, C., Beckmann, C.F., Bernard, A., Bertagnolli, D., Boe, A.F., Cartagena, P.M., Chakravarty, M.M., Chapin, M., Chong, J., Dalley, R.A., Daly, B.D., Dang, C., Datta, S., Dee, N., Dolbeare, T.A., Faber, V., Feng, D., Fowler, D.R., Goldy, J., Gregor, B.W., Haradon, Z., Haynor, D.R., Hohmann, J.G., Horvath, S., Howard, R.E., Jeromin, A., Jochim, J.M., Kinnunen, M., Lau, C., Lazarz, E.T., Lee, C., Lemon, T.A., Li, L., Li, Y., Morris, J.A., Overly, C.C., Parker, P.D., Parry, S.E., Reding, M., Royall, J.J., Schulkin, J., Sequeira, P.A., Slaughterbeck, C.R., Smith, S.C., Sodt, A.J., Sunkin, S. M., Swanson, B.E., Vawter, M.P., Williams, D., Wohnoutka, P., Zielke, H.R., Geschwind, D.H., Hof, P.R., Smith, S.M., Koch, C., Grant, S.G.N., Jones, A.R., 2012. An anatomically comprehensive atlas of the adult human brain transcriptome. Nature 489 (7416), 391–399.

He, L., Mäe, M.A., Muhl, L., Sun, Y., Pietilä, R., Nahar, K., Liébanas, E.V., Fagerlund, M. J., Oldner, A., Liu, J., Genové, G., Zhang, L., Xie, Y., Leptidis, S., Mocci, G., Stritt, S., Osman, A., Anisimov, A., Hemanthakumar, K.A., Räsänen, M., Mirabeau, O., Hansson, E., Björkegren, J., Vanlandewijck, M., Blomgren, K., Mäkinen, T., Peng, X. R., Arnold, T.D., Alitalo, K., Eriksson, L.I., Lendahl, U., Betsholtz, C., 2020. Pericyte-specific vascular expression of SARS-CoV-2 receptor ACE2 – implications for microvascular inflammation and hypercoagulopathy in COVID-19. bioRxiv 2020.05.11.088500. https://doi.org/10.1101/2020.05.11.088500.

L. Heijmans M.R. Mons E.A. Joosten A systematic review on descending serotonergic projections and modulation of spinal nociception in chronic neuropathic pain and after spinal cord stimulation Mol Pain 17 2021 10.1177/17448069211043965 174480692110439.

Hensley, M.K., Markantone, D., Prescott, H.C., 2022. Neurologic Manifestations and Complications of COVID-19. Annu. Rev. Med. 73 (1), 113–127.

Himberg, J., Hyvarinen, A., 2003. Icasso: software for investigating the reliability of ICA estimates by clustering and visualization, in: 2003 IEEE XIII Workshop on Neural Networks for Signal Processing (IEEE Cat. No.03TH8718). IEEE, pp. 259–268. https://doi.org/10.1109/NNSP.2003.1318025.

Horn, J.L., 1965. A rationale and test for the number of factors in factor analysis. Psychometrika 1965 30:2 30, 179–185. https://doi.org/10.1007/BF02289447.

Hosp, J.A., Dressing, A., Blazhenets, G., Bormann, T., Rau, A., Schwabenland, M., Thurow, J., Wagner, D., Waller, C., Niesen, W.D., Frings, L., Urbach, H., Prinz, M., Weiller, C., Schroeter, N., Meyer, P.T., 2021. Cognitive impairment and altered cerebral glucose metabolism in the subacute stage of COVID-19. Brain 144 (4), 1263–1276.

Hotelling, H., 1933. Analysis of a complex of statistical variables into principal components. J Educ Psychol 24, 417–441. https://doi.org/10.1037/H0071325.

Hui, M., Li, J., Wen, X., Yao, L., Long, Z., 2011. An empirical comparison of information-theoretic criteria in estimating the number of independent components of fMRI data. PloS One, e29274–e29274. https://doi.org/10.1371/journal.pone.0029274.

Iadecola, C., Anrather, J., Kamel, H., 2020. Effects of COVID-19 on the Nervous System. Cell 183 (1), 16–27.e1.

Iba, T., Connors, J.M., Levy, J.H., 2020. The coagulopathy, endotheliopathy, and vasculitis of COVID-19. Inflamm. Res. 69 (12), 1181–1189.

Jakobsen, J.C., Gluud, C., Wetterslev, J., Winkel, P., 2017. When and how should multiple imputation be used for handling missing data in randomised clinical trials - A practical guide with flowcharts. BMC Med Res Methodol 17, 1–10. https://doi.org/10.1186/S12874-017-0442-1/TABLES/2.

Jensen, K.E., Thomsen, C., Henriksen, O., 1988. In vivo measurement of intracellular pH in human brain during different tensions of carbon dioxide in arterial blood. A 31P-NMR study. Acta Physiol Scand 134, 295–298. https://doi.org/10.1111/j.1748-1716.1988.tb08492.x.

Kakarla, V., Kaneko, N., Nour, M., Khatibi, K., Elahi, F., Liebeskind, D.S., Hinman, J.D., 2021. Pathophysiologic mechanisms of cerebral endotheliopathy and stroke due to Sars-CoV-2 41, 1179–1192. https://doi.org/10.1177/0271678X20985666. https://doi.org/10.1177/0271678X20985666.

Kaneko, N., Satta, S., Komuro, Y., Muthukrishnan, S.D., Kakarla, V., Guo, L., An, J., Elahi, F., Kornblum, H.I., Liebeskind, D.S., Hsiai, T., Hinman, J.D., 2021. Flow-Mediated Susceptibility and Molecular Response of Cerebral Endothelia to SARS-CoV-2 Infection. Stroke 52 (1), 260–270.

Kannurpatti, S.S., Biswal, B.B., 2008. Detection and scaling of task-induced fMRI-BOLD response using resting state fluctuations. Neuroimage 40, 1567–1574. https://doi.org/10.1016/j.neuroimage.2007.09.040.

Keyeux, A., Ochrymowicz-Bemelmans, D., Charlier, A.A., 1995. Induced response to hypercapnia in the two-compartment total cerebral blood volume: influence on brain vascular reserve and flow efficiency. J Cereb Blood Flow Metab 15, 1121–1131. https://doi.org/10.1038/jcbfm.1995.139.

Khaddaj-Mallat, R., Aldib, N., Bernard, M., Paquette, A.-S., Ferreira, A., Lecordier, S., Saghatelyan, A., Flamand, L., ElAli, A., 2021. SARS-CoV-2 deregulates the vascular and immune functions of brain pericytes via Spike protein. Neurobiol Dis 161, 105561. https://doi.org/10.1016/J.NBD.2021.105561.

King, D.L.O., Henson, R.N., Kievit, R., Wolpe, N., Brayne, C., Tyler, L.K., Rowe, J.B., Cam-CAN, Tsvetanov, K.A., 2022. Distinct components of cardiovascular health are linked with age-related differences in cognitive abilities. medRxiv 2022.02.22.22271137. https://doi.org/10.1101/2022.02.22.22271137.

Kraha, A., Turner, H., Nimon, K., Zientek, L.R., Henson, R.K., 2012. Tools to Support Interpreting Multiple Regression in the Face of Multicollinearity. Front Psychol 3, 44. https://doi.org/10.3389/fpsyg.2012.00044.

Krishnan, A., Williams, L.J., McIntosh, A.R., Abdi, H., 2011. Partial Least Squares (PLS) methods for neuroimaging: A tutorial and review. Neuroimage 56, 455–475. https://doi.org/10.1016/j.neuroimage.2010.07.034.

Kroenke, K., Spitzer, R.L., Williams, J.B.W., 2001. The PHQ-9: validity of a brief depression severity measure. J Gen Intern Med 16, 606–613. https://doi.org/10.1046/J.1525-1497.2001.016009606.X.

Kroenke, K., Spitzer, R.L., Williams, J.B.W., 2002. The PHQ-15: validity of a new measure for evaluating the severity of somatic symptoms. Psychosom Med 64, 258–266. https://doi.org/10.1097/00006842-200203000-00008.

Lambertsen, C.J., Semple, S.J.G., Smyth, M.G., Gelfand, R., 1961. H$^+$ and pCO$_2$ as chemical factors in respiratory and cerebral circulatory control. J Appl Physiol 16, 473–484. https://doi.org/10.1152/jappl.1961.16.3.473.

Lassen, N.A., 1968. Brain extracellular pH: the main factor controlling cerebral blood flow. Scand J Clin Lab Invest 22, 247–251. https://doi.org/10.3109/00365516809167060.

Lersy, F., Anheim, M., Willaume, T., Chammas, A., Brisset, J.-C., Ois Cotton, F., Kremer, S., 2021. Cerebral vasculitis of medium-sized vessels as a possible mechanism of brain damage in COVID-19 patients. Journal of Neuroradiology 48, 141–146. https://doi.org/10.1016/j.neurad.2020.11.004.

Levi, M., Thachil, J., Iba, T., Levy, J.H., 2020. Coagulation abnormalities and thrombosis in patients with COVID-19. e440 Lancet Haematol 7, e438. https://doi.org/10.1016/S2352-3026(20)30145-9.

Li, Y.-O., Adali, T., Calhoun, V.D., 2007. Estimating the number of independent components for functional magnetic resonance imaging data. Human Brain Mapping 28 (11), 1251–1266. https://doi.org/10.1002/hbm.20359.

Liu, P., Li, Y., Pinho, M., Park, D.C., Welch, B.G., Lu, H., 2017. Cerebrovascular reactivity mapping without gas challenges. Neuroimage 146, 320–326. https://doi.org/10.1016/j.neuroimage.2016.11.054.

Liu, P., Liu, G., Pinho, M.C., Lin, Z., Thomas, B.P., Rundle, M., Park, D.C., Huang, J., Welch, B.G., Lu, H., 2021. Cerebrovascular Reactivity Mapping Using Resting-State BOLD Functional MRI in Healthy Adults and Patients with Moyamoya Disease. Radiology 299, 419–425. https://doi.org/10.1148/RADIOL.2021203568.

Liu, X., Tyler, L.K., Cam-Can, James, Rowe, B., Tsvetanov, K.A., 2022. Multimodal fusion analysis of functional, cerebrovascular and structural neuroimaging in healthy aging subjects. Hum Brain Mapp. https://doi.org/10.1002/HBM.26025.

Luan, Y.Y., Yin, C.H., Yao, Y.M., 2021. Update Advances on C-Reactive Protein in COVID-19 and Other Viral Infections. Front Immunol 12, 3153. https://doi.org/10.3389/FIMMU.2021.720363/BIBTEX.

Mahoney, F.I., Barthel, D.W., 1965. Barthel Index. Md State Med J 61–65.

Makedonov, I., Black, S.E., MacIntosh, B.J., Chao, L., 2013a. BOLD fMRI in the white matter as a marker of aging and small vessel disease. PLoS One 8 (7), e67652.

Makedonov, I., Black, S.E., MacIntosh, B.J., Chao, L., 2013b. BOLD fMRI in the white matter as a marker of aging and small vessel disease. PLoS One 8 (7), e67652.

Makedonov, I., Chen, J.J., Masellis, M., MacIntosh, B.J., 2016. Physiological fluctuations in white matter are increased in Alzheimer's disease and correlate with neuroimaging and cognitive biomarkers. Neurobiol Aging 37, 12–18. https://doi.org/10.1016/j.neurobiolaging.2015.09.010.

Marcic, M., Marcic, L., Marcic, B., Capkun, V., Vukojevic, K., 2021. Cerebral Vasoreactivity Evaluated by Transcranial Color Doppler and Breath-Holding Test in Patients after SARS-CoV-2 Infection. J Pers Med 11 (5), 379.

Marshall, J.C., Murthy, S., Diaz, J., Adhikari, N.K., Angus, D.C., Arabi, Y.M., Baillie, K., Bauer, M., Berry, S., Blackwood, B., Bonten, M., Bozza, F., Brunkhorst, F., Cheng, A., Clarke, M., Dat, V.Q., de Jong, M., Denholm, J., Derde, L., Dunning, J., Feng, X., Fletcher, T., Foster, N., Fowler, R., Gobat, N., Gomersall, C., Gordon, A., Glueck, T., Harhay, M., Hodgson, C., Horby, P., Kim, Y., Kojan, R., Kumar, B., Laffey, J., Malvey, D., Martin-Loeches, I., McArthur, C., McAuley, D., McBride, S., McGuinness, S., Merson, L., Morpeth, S., Needham, D., Netea, M., Oh, M.-D., Phyu, S., Piva, S., Qiu, R., Salisu-Kabara, H., Shi, L., Shimizu, N., Sinclair, J., Tong, S., Turgeon, A., Uyeki, T., van de Veerdonk, F., Webb, S., Williamson, P., Wolf, T., Zhang, J., 2020. A minimal common outcome measure set for COVID-19 clinical research. e197 Lancet Infect Dis 20, e192. https://doi.org/10.1016/S1473-3099(20)30483-7.

McGonagle, D., Bridgewood, C., Ramanan, A.V., Meaney, J.F.M., Watad, A., 2021a. COVID-19 vasculitis and novel vasculitis mimics. Lancet Rheumatol 3 (3), e224 e334.

McGonagle, D., Bridgewood, C., Ramanan, A.V., Meaney, J.F.M., Watad, A., 2021b. COVID-19 vasculitis and novel vasculitis mimics. Lancet Rheumatol 3 (3), e224–e233.

Millar, P.R., Ances, B.M., Gordon, B.A., Benzinger, T.L.S., Fagan, A.M., Morris, J.C., Balota, D.A., 2020a. Evaluating resting-state BOLD variability in relation to biomarkers of preclinical Alzheimer's disease. Neurobiol Aging 96, 233–245. https://doi.org/10.1016/J.NEUROBIOLAGING.2020.08.007.

Millar, P.R., Petersen, S.E., Ances, B.M., Gordon, B.A., Benzinger, T.L.S., Morris, J.C., Balota, D.A., 2020b. Evaluating the Sensitivity of Resting-State BOLD Variability to Age and Cognition after Controlling for Motion and Cardiovascular Inf luences: A Network-Based Approach. Cerebral Cortex 00, 1–16. https://doi.org/10.1093/cercor/bhaa138.

Millar, P.R., Ances, B.M., Gordon, B.A., Benzinger, T.L.S., Morris, J.C., Balota, D.A., 2021. Evaluating Cognitive Relationships with Resting-State and Task-driven Blood Oxygen Level-Dependent Variability. J Cogn Neurosci 33, 279–302. https://doi.org/10.1162/JOCN_A_01645.

Mitsikostas, D.D., Sanchez Del Rio, M., Waeber, C., 2002. 5-Hydroxytryptamine(1B/1D) and 5-hydroxytryptamine1F receptors inhibit capsaicin-induced c-fos immunoreactivity within mouse trigeminal nucleus caudalis. Cephalalgia 22, 384–394. https://doi.org/10.1046/J.1468-2982.2002.00382.X.

Mohkhedkar, M., Venigalla, S.S.K., Janakiraman, V., 2021. Autoantigens That May Explain Postinfection Autoimmune Manifestations in Patients With Coronavirus Disease 2019 Displaying Neurological Conditions. J Infect Dis 223, 536–537. https://doi.org/10.1093/INFDIS/JIAA703.

Nair, V.A., Raut, R.V., Prabhakaran, V., 2017. Investigating the Blood Oxygenation Level-Dependent Functional MRI Response to a Verbal Fluency Task in Early Stroke before and after Hemodynamic Scaling. Front Neurol 8, 283. https://doi.org/10.3389/fneur.2017.00283.

Nasreddine, Z.S., Phillips, N.A., Bédirian, V., Charbonneau, S., Whitehead, V., Collin, I., Cummings, J.L., Chertkow, H., 2005. The Montreal Cognitive Assessment, MoCA: a brief screening tool for mild cognitive impairment. J Am Geriatr Soc 53, 695–699. https://doi.org/10.1111/J.1532-5415.2005.53221.X.

Newcombe, V.F.J., Spindler, L.R.B., Das, T., Winzeck, S., Allinson, K., Stamatakis, E.A., Menon, D.K., Anwar, F., Bullmore, E., Coles, A., Coles, J., Jones, J., Lupson, V., Needham, E., Rowe, J., Sawcer, S., Valerio, F., 2021. Neuroanatomical substrates of generalized brain dysfunction in COVID-19. Intensive Care Med 47 (1), 116–118.

Nilsson, T., Longmore, J., Shaw, D., Jansen Olesen, I.J., Edvinsson, L., 1999. Contractile 5-HT1B receptors in human cerebral arteries: pharmacological characterization and localization with immunocytochemistry. Br J Pharmacol 128, 1133–1140. https://doi.org/10.1038/SJ.BJP.0702773.

Nimon, K., Lewis, M., Kane, R., Haynes, R.M., 2008. An R package to compute commonality coefficients in the multiple regression case: An introduction to the package and a practical example. Behav Res Methods 40, 457–466. https://doi.org/10.3758/BRM.40.2.457.

Passamonti, L., Tsvetanov, K.A., Jones, P.S., Bevan-Jones, W.R., Arnold, R., Borchert, R.J., Mak, E., Su, L., O'Brien, J.T., Rowe, J.B., 2019. Neuroinflammation and functional connectivity in Alzheimer's disease: interactive influences on cognitive performance. The Journal of Neuroscience 39, 2574–12518. https://doi.org/10.1523/jneurosci.2574-18.2019.

Paterson, R.W., Brown, R.L., Benjamin, L., Nortley, R., Wiethoff, S., Bharucha, T., Jayaseelan, D.L., Kumar, G., Raftopoulos, R.E., Zambreanu, L., Vivekanandam, V., Khoo, A., Geraldes, R., Chinthapalli, K., Boyd, E., Tuzlali, H., Price, G., Christofi, G., Morrow, J., McNamara, P., McLoughlin, B., Lim, S.T., Mehta, P.R., Levee, V., Keddie, S., Yong, W., Trip, S.A., Foulkes, A.J.M., Hotton, G., Miller, T.D., Everitt, A. D., Carswell, C., Davies, N.W.S., Yoong, M., Attwell, D., Sreedharan, J., Silber, E., Schott, J.M., Chandratheva, A., Perry, R.J., Simister, R., Checkley, A., Longley, N.,

Farmer, S.F., Carletti, F., Houlihan, C., Thom, M., Lunn, M.P., Spillane, J., Howard, R., Vincent, A., Werring, D.J., Hoskote, C., Jäger, H.R., Manji, H., Zandi, M. S., 2020. The emerging spectrum of COVID-19 neurology: clinical, radiological and laboratory findings. Brain 143 (10), 3104–3120.

Pearson, K., 1901. On lines and planes of closest fit to systems of points in space. The London, Edinburgh, and Dublin Philosophical Magazine and Journal of Science 2, 559–572. https://doi.org/10.1080/14786440109462720.

Pruim, R.H.R., Mennes, M., Buitelaar, J.K., Beckmann, C.F., 2015a. Evaluation of ICA-AROMA and alternative strategies for motion artifact removal in resting state fMRI. Neuroimage 112, 278–287. https://doi.org/10.1016/j.neuroimage.2015.02.063.

Pruim, R.H.R., Mennes, M., van Rooij, D., Llera, A., Buitelaar, J.K., Beckmann, C.F., 2015b. ICA-AROMA: A robust ICA-based strategy for removing motion artifacts from fMRI data. Neuroimage 112, 267–277. https://doi.org/10.1016/j.neuroimage.2015.02.064.

Rissanen, J., 1978. Modeling by shortest data description. Automatica 465–471. https://doi.org/10.1016/0005-1098(78)90005-5.

Rostrup, E., Larsson, H.B.W., Toft, P.B., Garde, K., Thomsen, C., Ring, P., Søndergaard, L., Henriksen, O., 1994. Functional MRI of CO2 induced increase in cerebral perfusion. NMR Biomed 7, 29–34. https://doi.org/10.1002/nbm.1940070106.

Rostrup, E., Larsson, H.B.W., Toft, P.B., Garde, K., Ring, P.B., Henriksen, O., 1996. Susceptibility Contrast Imaging of CO_2-Induced Changes in the Blood Volume of the Human Brain. Acta radiol 37, 813–822. https://doi.org/10.3109/02841859609177722.

Schnaubelt, S., Oppenauer, J., Tihanyi, D., Mueller, M., Maldonado-Gonzalez, E., Zejnilovic, S., Haslacher, H., Perkmann, T., Strassl, R., Anders, S., Stefenelli, T., Zehetmayer, S., Koppensteiner, R., Domanovits, H., Schlager, O., 2021. Arterial stiffness in acute COVID-19 and potential associations with clinical outcome. J Intern Med 290, 437–443. https://doi.org/10.1111/JOIM.13275.

Secchinato, K.F., da Silva, P.H.R., Camargo, A.P.A., Pontes-Neto, O.M., Leoni, R.F., 2019. Cerebrovascular reactivity mapping without hypercapnic challenge in patients with carotid artery stenosis. Revista Brasileira de Física Médica 13, 62–65. https://doi.org/10.29384/RBFM.2019.V13.N2.P62-65.

Shi, Y., Thrippleton, M.J., Makin, S.D., Marshall, I., Geerlings, M.I., de Craen, A.J.M., van Buchem, M.A., Wardlaw, J.M., 2016. Cerebral blood flow in small vessel disease: A systematic review and meta-analysis. J Cereb Blood Flow Metab 36, 1653–1667. https://doi.org/10.1177/0271678X16662891.

Sibille, E., Su, J., Leman, S., le Guisquet, A.M., Ibarguen-Vargas, Y., Joeyen-Waldorf, J., Glorioso, C., Tseng, G.C., Pezzone, M., Hen, R., Belzung, C., 2007. Lack of serotonin1B receptor expression leads to age-related motor dysfunction, early onset of brain molecular aging and reduced longevity. Mol Psychiatry 12, 1042–1056. https://doi.org/10.1038/SJ.MP.4001990.

Spitzer, R.L., Kroenke, K., Williams, J.B.W., Löwe, B., 2006. A brief measure for assessing generalized anxiety disorder: the GAD-7. Arch Intern Med 166, 1092–1097. https://doi.org/10.1001/ARCHINTE.166.10.1092.

Swinson, R.P., 2006. The GAD-7 scale was accurate for diagnosing generalised anxiety disorder. Evid Based Med 11 (6), 184.

Taneja, K., Lu, H., Welch, B.G., Thomas, B.P., Pinho, M., Lin, D., Hillis, A.E., Liu, P., 2019. Evaluation of cerebrovascular reserve in patients with cerebrovascular diseases using resting-state MRI: A feasibility study. Magn Reson Imaging 59, 46–52. https://doi.org/10.1016/J.MRI.2019.03.003.

Tsvetanov, K.A., Henson, R.N.A., Tyler, L.K., Davis, S.W., Shafto, M.A., Taylor, J.R., Williams, N., Rowe, J.B., 2015. The effect of ageing on fMRI: Correction for the confounding effects of vascular reactivity evaluated by joint fMRI and MEG in 335 adults. Hum Brain Mapp 36, 2248–2269. https://doi.org/10.1002/hbm.22768.

Tsvetanov, K.A., Henson, R.N.A., Tyler, L.K., Razi, A., Geerligs, L., Ham, T.E., Rowe, J.B., 2016. Extrinsic and intrinsic brain network connectivity maintains cognition across the lifespan despite accelerated decay of regional brain activation. Journal of Neuroscience 36 (11), 3115–3126.

Tsvetanov, K.A., Ye, Z., Hughes, L., Samu, D., Treder, M.S., Wolpe, N., Tyler, L.K., Rowe, J.B., for Cambridge Centre for Ageing and Neuroscience,, 2018. Activity and connectivity differences underlying inhibitory control across the adult lifespan. J Neurosci 38, 7887–7900. https://doi.org/10.1523/JNEUROSCI.2919-17.2018.

Tsvetanov, K.A., Gazzina, S., Jones, P.S., Swieten, J., Borroni, B., Sanchez-Valle, R., Moreno, F., Laforce, R., Graff, C., Synofzik, M., Galimberti, D., Masellis, M., Tartaglia, M.C., Finger, E., Vandenberghe, R., Mendonça, A., Tagliavini, F., Santana, I., Ducharme, S., Butler, C., Gerhard, A., Danek, A., Levin, J., Otto, M., Frisoni, G., Ghidoni, R., Sorbi, S., Rohrer, J.D., Rowe, J.B., Afonso, S., Almeida, M.R., Anderl-Straub, S., Andersson, C., Antonell, A., Archetti, S., Arighi, A., Balasa, M., Barandiaran, M., Bargalló, N., Bartha, R., Bender, B., Benussi, A., Bessi, V., Binetti, G., Black, S., Bocchetta, M., Borrego-Ecija, S., Bras, J., Bruffaerts, R., Caroppo, P., Cash, D., Castelo-Branco, M., Convery, R., Cope, T., Cosseddu, M., de Arriba, M., Di Fede, G., Díaz, Z., Moore, K.M., Duro, D., Fenoglio, C., Ferrari, C., Ferreira, C., Ferreira, C.B., Flanagan, T., Fox, N., Freedman, M., Fumagalli, G., Gabilondo, A., Gasparotti, R., Gauthier, S., Gazzina, S., Giaccone, G., Gorostidi, A., Greaves, C., Guerreiro, R., Heller, C., Hoegen, T., Indakoetxea, B., Jelic, V., Jiskoot, L., Karnath, H.-O., Institutet, K., Keren, R., Langheinrich, T., Leitão, M.J., Lladó, A., Lombardi, G., Loosli, S., Maruta, C., Mead, S., Meeter, L., Miltenberger, G., van Minkelen, R., Mitchell, S., Nacmias, B., Neason, M., Nicholas, J., Olives, J., Padovani, A., Panman, J., Papma, J., Piaceri, I., Pievani, M., Pijnenburg, Y., Polito, C., Premi, E., Prioni, S., Prix, C., Rademakers, R., Redaelli, V., Rittman, T., Rogaeva, E., Rosa-Neto, P., Rossi, G., Rossor, M., Santiago, B., Scarpini, E., Schönecker, S., Semler, E., Shafei, R., Shoesmith, C., Tábuas-Pereira, M., Tainta, M., Taipa, R., Tang-Wai, D., Thomas, D.L., Thompson, P., Thonberg, H., Timberlake, C., Tiraboschi, P., Vandamme, P., Vandenbulcke, M., Veldsman, M., Verdelho, A., Villanua, J., Warren, J., Wilke, C., Woollacott, I., Wlasich, E., Zetterberg, H., Zulaica, M., 2021a. Brain functional network integrity sustains cognitive function

despite atrophy in presymptomatic genetic frontotemporal dementia. Alzheimer's & Dementia 17 (3), 500–514.

Tsvetanov, K.A., Henson, R.N.A., Jones, P.S., Mutsaerts, H., Fuhrmann, D., Tyler, L.K., Rowe, J.B., 2021b. The effects of age on resting-state BOLD signal variability is explained by cardiovascular and cerebrovascular factors. Psychophysiology 58 (7). https://doi.org/10.1111/psyp.13714.

Tsvetanov, K.A., Henson, R.N.A., Rowe, J.B., 2021c. Separating vascular and neuronal effects of age on fMRI BOLD signals. Philosophical Transactions of the Royal Society B: Biological Sciences. 376 (1815), 20190631.

Ulhaq, Z.S., Soraya, G.V., 2020. Interleukin-6 as a potential biomarker of COVID-19 progression. Med Mal Infect 50, 382–383. https://doi.org/10.1016/J.MEDMAL.2020.04.002.

Vaishnavi, S.N., Vlassenko, A.G., Rundle, M.M., Snyder, A.Z., Mintun, M.A., Raichle, M.E., 2010. Regional aerobic glycolysis in the human brain. Proc Natl Acad Sci U S A 107, 17757–17762. https://doi.org/10.1073/PNAS.1010459107/-/DCSUPPLEMENTAL.

van Buuren, S., Groothuis-Oudshoorn, K., 2011. mice: Multivariate Imputation by Chained Equations in R. J Stat Softw 45, 1–67. https://doi.org/10.18637/JSS.V045.I03.

van der Maaten, L.J.P., Postma, E.O., van den Herik, H.J., 2009. Dimensionality reduction: A comparative review. Technical Report TiCC-TR 2009–2025.

Verity, R., Okell, L.C., Dorigatti, I., Winskill, P., Whittaker, C., Imai, N., Cuomo-Dannenburg, G., Thompson, H., Walker, P.G.T., Fu, H., Dighe, A., Griffin, J.T., Baguelin, M., Bhatia, S., Boonyasiri, A., Cori, A., Cucunubá, Z., FitzJohn, R., Gaythorpe, K., Green, W., Hamlet, A., Hinsley, W., Laydon, D., Nedjati-Gilani, G., Riley, S., van Elsland, S., Volz, E., Wang, H., Wang, Y., Xi, X., Donnelly, C.A., Ghani, A.C., Ferguson, N.M., 2020. Estimates of the severity of coronavirus disease 2019: a model-based analysis. Lancet Infect Dis 20, 669–677. https://doi.org/10.1016/S1473-3099(20)30243-7/ATTACHMENT/E32585C1-0F24-46F4-855E-FC2C52BBAFD7/MMC1.PDF.

Vestergaard, M.B., Jensen, M.LF., Arngrim, N., Lindberg, U., Larsson, H.BW., 2020. Higher physiological vulnerability to hypoxic exposure with advancing age in the human brain. Journal of Cerebral Blood Flow & Metabolism 40 (2), 341–353.

Vlassenko, A.G., Vaishnavi, S.N., Couture, L., Sacco, D., Shannon, B.J., Mach, R.H., Morris, J.C., Raichle, M.E., Mintun, M.A., 2010. Spatial correlation between brain aerobic glycolysis and amyloid-β (Aβ) deposition. Proc Natl Acad Sci U S A 107, 17763–17767. https://doi.org/10.1073/PNAS.1010461107.

Wagerle, L.C., Mishra, O.P., 1988. Mechanism of CO2 response in cerebral arteries of the newborn pig: Role of phospholipase, cyclooxygenase, and lipoxygenase pathways. Circ Res 62, 1019–1026. https://doi.org/10.1161/01.RES.62.5.1019.

Ware, J.E., Sherbourne, C.D., 1992. The MOS 36-ltem Short-Form Health Survey (SF-36). Med Care 30 (6), 473–483.

Willie, C.K., Tzeng, Y.-C., Fisher, J.A., Ainslie, P.N., 2014. Integrative regulation of human brain blood flow. J Physiol 592, 841–859. https://doi.org/10.1113/jphysiol.2013.268953.

Wool, G.D., Miller, J.L., 2021. The Impact of COVID-19 Disease on Platelets and Coagulation. Pathobiology 88, 15–27. https://doi.org/10.1159/000512007.

Wu, S., Tyler, L.K., Henson, R.N.A., Rowe, J.B., Cam-CAN, Tsvetanov, K.A., 2021. Cerebral blood flow predicts multiple demand network activity and fluid intelligence across the lifespan. bioRxiv 2021.11.10.468042-2021.11.10.468042. https://doi.org/10.1101/2021.11.10.468042.

Wu, S., Tyler, L.K., Henson, R.N.A., Rowe, J.B., Cam-CAN, Tsvetanov, K.A., 2023. Cerebral blood flow predicts multiple demand network activity and fluid intelligence across the adult lifespan. Neurobiol Aging 121, 1–14.

Xu, J., Potenza, M.N., Calhoun, V.D., 2013. Spatial ICA reveals functional activity hidden from traditional fMRI GLM-based analyses. Front Neurosci 7, 1–4. https://doi.org/10.3389/fnins.2013.00154.

Yang, A.C., Vest, R.T., Kern, F., Lee, D.P., Maat, C.A., Losada, P.M., Chen, M.B., Agam, M., Schaum, N., Khoury, N., Calcuttawala, K., Pálovics, R., Shin, A., Wang, E.Y., Luo, J., Gate, D., Siegenthaler, J.A., McNerney, M.W., Keller, A., Wyss-Coray, T., 2021. A human brain vascular atlas reveals diverse cell mediators of Alzheimer's disease risk. bioRxiv 2021.04.26.441262. https://doi.org/10.1101/2021.04.26.441262.

Zhang, X.-J., Qin, J.-J., Cheng, X.u., Shen, L., Zhao, Y.-C., Yuan, Y., Lei, F., Chen, M.-M., Yang, H., Bai, L., Song, X., Lin, L., Xia, M., Zhou, F., Zhou, J., She, Z.-G., Zhu, L., Ma, X., Xu, Q., Ye, P., Chen, G., Liu, L., Mao, W., Yan, Y., Xiao, B., Lu, Z., Peng, G., Liu, M., Yang, J., Yang, L., Zhang, C., Lu, H., Xia, X., Wang, D., Liao, X., Wei, X., Zhang, B.-H., Zhang, X., Yang, J., Zhao, G.-N., Zhang, P., Liu, P.P., Loomba, R., Ji, Y.-X., Xia, J., Wang, Y., Cai, J., Guo, J., Li, H., 2020. In-Hospital Use of Statins Is Associated with a Reduced Risk of Mortality among Individuals with COVID-19. Cell Metab 32 (2), 176–187.e4.

Zubair, A.S., McAlpine, L.S., Gardin, T., Farhadian, S., Kuruvilla, D.E., Spudich, S., 2020. Neuropathogenesis and Neurologic Manifestations of the Coronaviruses in the Age of Coronavirus Disease 2019: A Review. JAMA Neurol 77, 1018–1027. https://doi.org/10.1001/JAMANEUROL.2020.2065.